2009

ROMP-based polymer composites and biorenewable rubbers

Wonje Jeong
Iowa State University

ROMP-based polymer composites and biorenewable rubbers

by

Wonje Jeong

A dissertation submitted to the graduate faculty

in partial fulfillment of the requirements for the degree of

DOCTOR OF PHILOSOPHY

Major: Materials Science and Engineering

Program of Study Committee:
Michael R. Kessler, Major Professor
Scott Chumbley
Zhiqun Lin
David Grewell
Malika Jeffries-EL

Iowa State University

Ames, Iowa

2009

TABLE OF CONTENTS

LIST OF FIGURES

LIST OF TABLES

ACKNOWLEDGEMENTS

I would like to sincerely thank my advisor, Dr. Michael R. Kessler. The completion of this work would not be achieved without his guidance and encouragement throughout the research process. I would also like to thank Dr. Scott Chumbley, Dr. Zhiqun Lin, Dr. David Grewell, and Dr. Malika Jeffries-EL for serving on my advisory committee and providing additional technical guidance.

I would like to give great thanks to current and former members of the polymer composites research group—Xia Sheng, Timothy C. Mauldin, William Kirby Goertzen, and Louis Charles—for their valuable discussions and their support throughout my research. I would also like to extend thanks to Goknur Tutuncu, Mesut Varlioglu, Jun Wang, Marlin Valverde for their technical advice and help. I would like to give deep thanks to my Korean friends in the Materials Science and Engineering Department at Iowa State University, who have shared valuable memories during my 5 years in Ames, IA. I would also like to give special thanks to my mentor and role model, Dr. Sanghoon Lee for continuous motivation.

Finally, I need to express my extreme gratitude to my parents and family for their unwavering love, support, and encouragement throughout this whole process. Without them, I never would have completed this research.

ABSTRACT

This research is divided into two related topics. In the first topic, the synthesis and characterization of novel composite materials reinforced with MWCNTs by ring-opening metathesis polymerization (ROMP) is reported for two ROMP based monomers: dicyclopentadiene (DCPD) and 5-ethylidene-2-norbornene (ENB). Homogeneous dispersion of MWCNTs in the polymer matrices is achieved by grafting norbornene moieties onto the nanotube surface. For the DCPD-based system, the investigation of mechanical properties of the composites shows a remarkable increase of tensile toughness with just 0.4 wt % of functionalized MWCNTs (f-MWCNTs). To our knowledge, this represents the highest toughness enhancement efficiency in thermosetting composites ever reported. DMA results show that there is a general increase of thermal stability (T_g) with the addition of f-MWCNTs, which means that covalently bonded f-MWCNTs can reduce the local chain mobility of the matrix by interfacial interactions. The ENB system also shows significant enhancement of the toughness using just 0.8 wt % f-MWCNTs. These results indicate that the ROMP approach for polyENB is also very effective.

The second topic is an investigation of the biorenewable rubbers synthesized by the tandem ROMP and cationic polymerization. The resin consists of a norbornenyl-modified linseed oil and a norbornene diester. Characterization of the bio-based rubbers includes dynamic mechanical analysis, tensile testing, and thermogravimetric analysis. The experimental results show that there is a decrease in glass transition temperature and slight increase of elongation with increased diester loading.

CHAPTER 1: GENERAL INTRODUCTION

1.1 Introduction

This thesis consists of two parts: Multiwalled carbon nanotube reinforced polymer composites and bio-based rubber composites.

1.1.1 Multiwall carbon nanotube (MWCNT) reinforced polymer composites

Polymer nanocomposites (PNCs) have been studied intensively by both academia and industry for the past 20 years, and this research has grown exponentially over that time. In contrast to conventional composites, where the size of the reinforcement is on the order of microns, the advantage of PNCs is not simply based on the mechanical enhancement of the neat resin or the direct replacement of current microscale filler. Rather, it provides multi-functional properties which are not present in the neat resin, often without sacrificing the resin's inherent properties, or adding excessive weight.

The first report of polymer nanocomposites using carbon nanotubes (CNTs) as filler was in the mid 90's in an epoxy matrix [1]. Since that time there have been over 9,900 papers written on the topic of polymer nanocomposites [2]. The high strength, modulus and large aspect ratio of carbon nanotubes, combined with superlative electrical, magnetic, optical and thermal properties make nanotubes attractive candidates for multifunctional nano-reinforced polymer composites [3]. However the non-reactive surface and strong aggregative properties has limited the utilities of CNTs for many matrices. In order to use the unique multifunctional properties of CNTs for effective reinforcement, well-dispersed nanotubes with good adhesion throughout the polymer matrix is a prerequisite [4,5]. A number of surface-functionalization techniques have been proposed to modify the intrinsic properties of

nanotubes for tailoring the nanotube surface for optimized properties. There are two strategic approaches for carbon nanotube/polymer composites: The “grafting to” approach which involves reactions of growing polymer molecules having reactive end groups with functional groups on the nanotube surface [6,7] and the “grafting from” approach which initiates reactions from an initiator or reactive groups covalently attached to the nanotube surface [8,9].

With the recent development of ruthenium based catalysts for olefin metathesis which are tolerant of a wide range of polar functionalities, the ring-opening metathesis polymerization (ROMP) has recently emerged as a powerful tool to synthesize well-defined macromolecular materials [10-13]. ROMP also has been developed for synthetic protocols for the modification of inorganic surfaces such as silica [14], silicon [15,16], and gold [17-19]: both “grafting from” and “grafting to” approaches are applied to polymerize to and from the surface.

Another importance of ROMP is the production of industrially applicable polymers. Two promising ROMP monomers are dicyclopentadiene (DCPD) and 5-ethylidene-2-norbornene (ENB). DCPD has received much attention as a monomer for ROMP due to its high modulus, excellent impact strength, and chemical resistance [20]. It can be polymerized via ROMP giving polyDCPD which is used in high performance structures as a matrix material [21]. In order to use DCPD for a composite matrix it is necessary that fillers to be modified to be compatible with the highly nonpolar hydrophobic properties of DCPD. ENB, which polymerizes into a linear polymer (in contrast to the polymer network that results from DCPD), also has excellent thermomechanical properties and polymerizes much more rapidly than DCPD.

The goal of this research is to develop MWCNT reinforced polymer composites by ROMP with DCPD and ENB. The issue of dispersion, load transfer, and interfacial interactions is controlled by functionalizing MWCNTs. The fabrication of functionalized MWCNT reinforced polymer composites by ROMP with different nanotube loadings is developed and the evaluation of the influence of nanotubes on the thermal and mechanical properties of these composites is investigated.

1.1.2 Biorenewable rubbers

The primary uses for rubbers in the transportation industry are seals, tubing, and tires. Tires represent the largest use. Synthetic rubber constitutes 14-28% of the composition of tires. These rubbers are combined with appropriate fillers, such as carbon black and silica to form a composite for enhanced mechanical integrity and improved durability. Not only do these rubbers rely on diminishing fossil fuels, they also create a significant negative impact on the environment (shortage of landfill space, emissions resulting from incineration, and hazards to human and animal health). The Rubber manufacturers Association estimates that 2-3 billion scrap tires are present in landfills or are otherwise "stockpiled" across the U.S. in roadside dumps, rural lots, and warehouses.

Bio-renewable polymers are quickly becoming viable alternatives to petroleum-based plastics, and offer improved biodegradation at the end of their service life. Substantial progress in the development of biopolymers and rubbers derived from soybean, corn and linseed oils has occurred over the last decade [22-26].

Replacing synthetic rubbers used in tires with bio-renewable rubber composites would have two major advantages: 1) development of a large market for bio-renewable rubbers, hence decreasing the dependence on petroleum and 2) reduction of the

environmental impact imposed by scrap tires by potentially improving the long term biodegradability of tires.

The goal of this research is to develop novel bio-based rubbers from modified linseed oil by combination of both cationic polymerization and ring-opening metathesis polymerization. The research is focused on the synthesis and characterization of bio-based rubbers and the evaluation of their thermal and mechanical properties.

1.2 Dissertation organization

This work is organized into main chapters, which are each manuscripts that have either been published in or prepared for submission to scholarly journals.

Chapter 1 gives a general introduction that outlines the background and motivation of the two main topics: developing MWCNT reinforced polymer composites by ROMP and bio-based rubbers polymerized by both ROMP and cationic polymerization of a modified vegetable oil. Chapter 1 also includes a short introduction to the mechanism of ROMP of DCPD followed by a detailed introduction to functionalize MWCNTs. Finally, a brief discussion of the structure of vegetable oils is also introduced.

Chapter 2 involves the development of norbornene funtionalized MWCNT (f-MWCNT) reinforced polyDCPD composites. A remarkable increase of tensile toughness (925%) with the addition of just 0.4 wt % functionalized MWCNTs was achieved, along with increasing thermal stability.

Chapter 3 also involves fabrication of f-MWCNT reinforced polyENB thermoplastics by ROMP. An increase in tensile toughness of over 300% is achieved with a loading of just 0.8 wt % of the f-MWCNTs. This increased toughness is believed to be a result of strong

interactions that develop between the norbornene functional groups on the surface of the nanotubes and the polymer matrix during ROMP.

Chapter 4 includes the synthesis and characterization of bio-based rubbers by simultaneous cationic polymerization and ROMP. An ester derivative of bicyclohept-2-ene, which was synthesized and copolymerized with a norbornenyl-modified linseed oil, is added to decrease the glass transition temperature and increase the elongation at break for the resulting rubber. The overall thermal-mechanical properties are investigated in detail by dynamic mechanical analysis, tensile testing, and thermogravimetric analysis.

Chapter 5 provides general discussions of conclusions drawn and provides suggestions for future work.

1.3 Background and literature review

1.3.1 Ring-opening metathesis polymerization

ROMP is a chain growth polymerization process where a mixture of cyclic olefin is converted to a polymeric material [27]. The mechanism of the polymerization is based on olefin metathesis, a unique metal-mediated carbon-carbon double bond exchange process [28]. As a result, any unsaturation associated with the monomer is conserved as it is converted to polymer. This is an important feature that distinguishes ROMP from typical olefin addition polymerizations (e.g. ethylene → polyethylene).

The polymerization of cyclic, strained olefins by transition metal alkylidenes of general formula $L_nM = CRR'$ (L = ligand, R, R' = H, alkyl, aryl) yields polymers via ring-opening that contain unsaturated double bonds within each repetitive unit. Since the

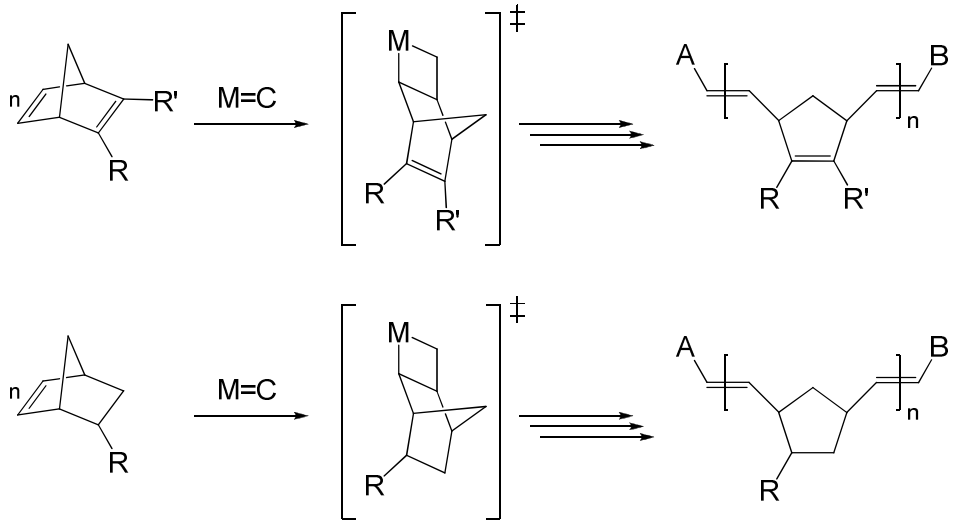

Figure 1-1ROMP of a 2,3-disubstituted norbornadiene and a 2-substituted norborn-5-ene [26].

mechanism is based on repetitive metathesis steps, this polymerization reaction is known as "ring-opening metathesis polymerization". Olefins with cyclic, or bi- or tricyclic strained ring structures (norborn-2-enes or norbornadienes for instance) are required (Figure 1-1).

1.3.2 Grubbs' catalyst

The advances in ROMP can be attributed to tremendous efforts by a large number of researchers focusing on the development of well-defined, functional group tolerant catalysts accessible to olefin metathesis. Early catalyst systems were extremely sensitive toward air and moisture, difficult to characterize, and difficult to systematically study and optimize. So it was recognized (with a Nobel Prize in 2006) that the development of a catalyst with a well-defined structure was essential for olefin metathesis.

In any catalyst system, functional groups in the substrate or solvent (including oxygen and water) can interfere with catalytic activity in several ways. Thus, the key to improved functional group tolerance in olefin metathesis is the development of a catalyst that reacts preferentially with olefins in the presence of heteroatomic functionalities. Ruthenium based catalysts react preferentially with carbon-carbon double bonds over most other species, which makes these catalysts unusually stable toward alcohols, amides, aldehydes, and carboxylic acids (Table 1-1) [29].

1.3.3 Ring-opening metathesis polymerization of dicyclopentadiene

The polymerization initiated by the ruthenium/alkylidene complex (Grubbs' catalyst) of DCPD is highly exothermic because of the relief of ring strain energy. Figure 1-2 illustrates the ROMP mechanism for the DCPD system. First the ruthenium metal carbene and the cycloalkene combine to form an intermediate metallacyclobutane. The metallacycle then breaks between the atoms that initially shared a double bond and the new olefin that is

Table.1-1 Functional group tolerance of early and late transition metal olefin metathesis catalysts.

Titanium	**Tungsten**	**Molybdenum**	**Ruthenium**	
Acids	Acids	Acids	**Olefins**	
Alcohols,	Alcohols,	Alcohols,	Acids	
Water	Water	Water		
Aldehydes	Aldehydes	Aldehydes	Alcohols,	Increasing
			Water	
Ketones	Ketones	**Olefins**	Aldehydes	Reactivity
Ester, Amides	**Olefins**	Ketones	Ketones	
Olefins	Ester, Amides	Ester, Amides	Ester, Amides	

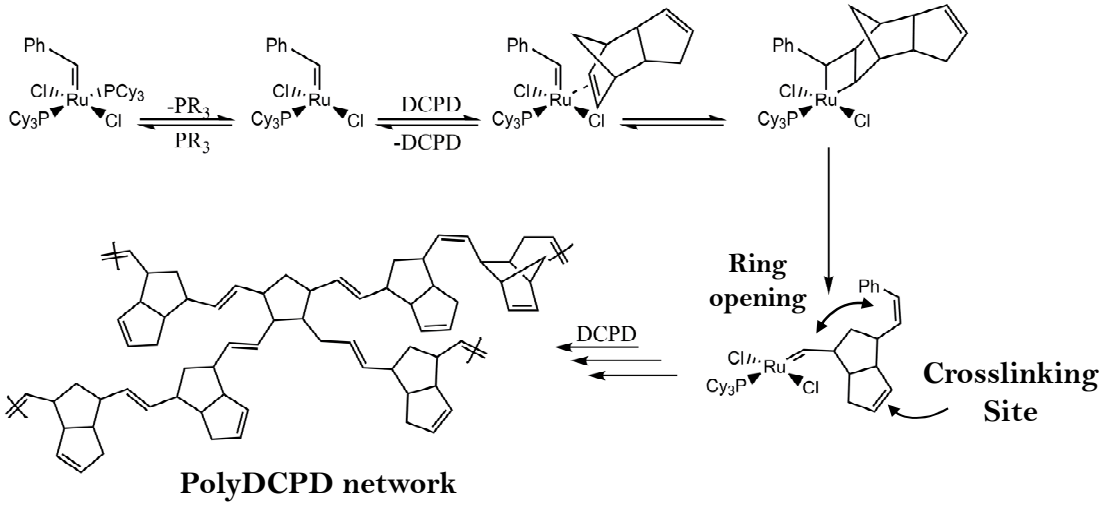

Figure 1-2 Ring-opening metathesis of polymerization of dicyclopentadiene

generated remains attached to the catalyst as part of a growing polymer chain. The remaining double bond may be polymerized in a similar way to form a cross-linked poly-DCPD network.

1.3.4 Functionalization of carbon nanotubes

In the past decade, significant progress has been made in the area of functionalization of carbon nanotubes using various chemistries. Functionalization of nanotubes is a prerequisite for further applications since CNTs are often non-compatible with solution chemistry. Functionalization of CNTs with interesting polymers has been recognized as one of the most promising approaches to the formation of nanocomposites. By taking advantage of the solubility and processability of the product, the resulting materials will not only provide a good matrix, but will also retain the high mechanical strength and electronic conductivity of CNTs. These materials have great potential for use in different applications, including materials for space shuttles and organic electronic devices. A vast number of studies have been reported on polymer-based CNT derivatives, where CNTs were used as a support for polymerization or for organic reactions. A series of successful functionalization reactions have been accomplished by different types of approaches such as indirect covalent functionalization, direct covalent functionalization, and non-covalent functionalization.

Oxidatively modified CNTs can be obtained by using strong acids such as nitric acid, or other strong oxidizing agents during purification processing. Various functionalities have been reported depending on the processing conditions, including ketone, alcohol, and ester groups [30]. This processing also leads to a shortening of the tubes with oxidized groups located at the tips, as well as on the walls. The first report of successful chemistry with CNTs

was reported by the Smalley group [31], which involved a treatment under strong acidic conditions such as sonication in a mixture of sulfuric and nitric acid.

The introduction of carboxylic acid functionalities at the tube ends and side wall during the oxidation purification process provides starting points for amidation and acylation of these oxidized tubes. The development of the surface chemistry has stimulated many studies on the further derivatization of oxidized CNTs with different moieties. Figure 1-3 shows the schematics of indirect covalent functionalization routes used to derivatize CNTs at defect sites.

An alternative sidewall functionalization of carbon nanotubes, which eliminates the need for acid pretreatment, has been achieved recently. The chemical reactivity in strained carbon systems arises from two factors: a) pyramidalization at the carbon atom, and b) π-orbital misalignment between adjacent carbon atoms. In CNTs, π-orbital misalignment is expected to have a greater influence rather than the pyramidalization strain. The functionalization of sidewalls by covalent bond has been achieved by a highly reactive reagent. There are numerous different approaches for direct covalent functionalization onto the nanotube surface: (a) Halogenation, (b) Hydrogenation, (c) Arylation, (d) Amination, (e) Cycloaddition, (f) Addition of Nitrenes, Carbenes, and Radicals.

The surface of CNTs can be noncovalently wrapped by various species of polymers, polynuclear aromatic compounds, surfactant, and biomolecules. Noncovalent functionalization of CNT is attractive because it offers the possibility of attaching chemical functionalities without affecting the electronic network of the tubes and disrupting the bonding network of nanotubes [32].

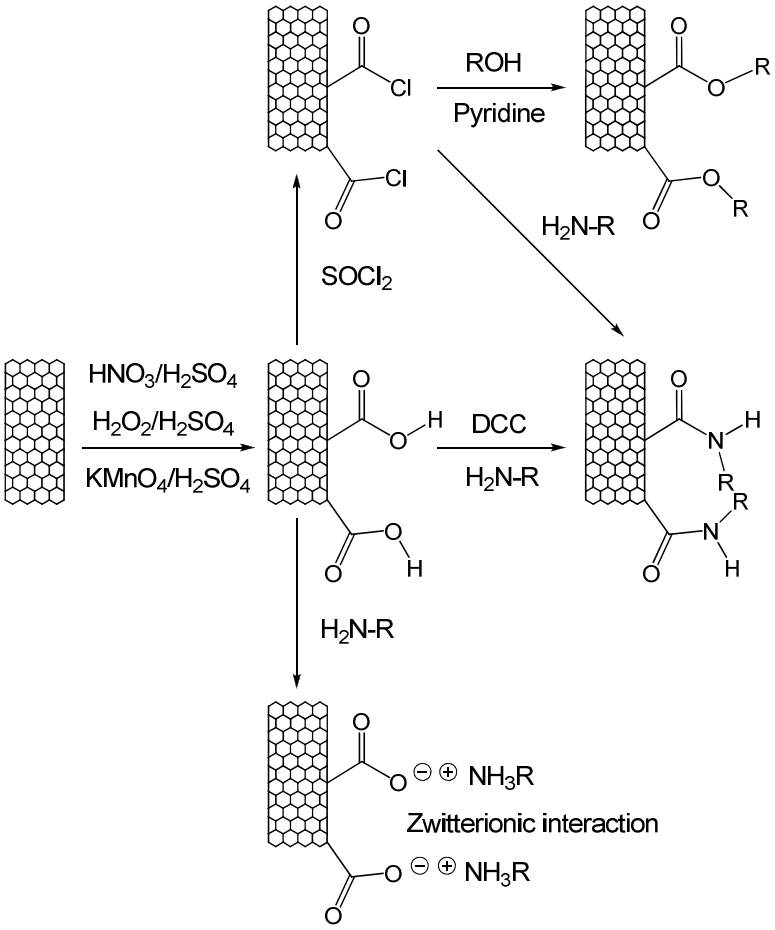

Figure 1-3 Schematics of functionalization routes used to derivatize CNT at defect site.

1.3.5 Natural Oils

Natural oils are triglyceride esters of fatty acids and the structure is shown in Figure 1-4. Triglycerides comprise three fatty acids joined by a glycerol center. The oils contain fatty acids that vary from 14 to 22 carbons in length with 1 to 3 double bonds. The fatty acid distribution of several oils is shown in Table 1-2, which shows that there are many different types of triglycerides with numerous levels of unsaturation.

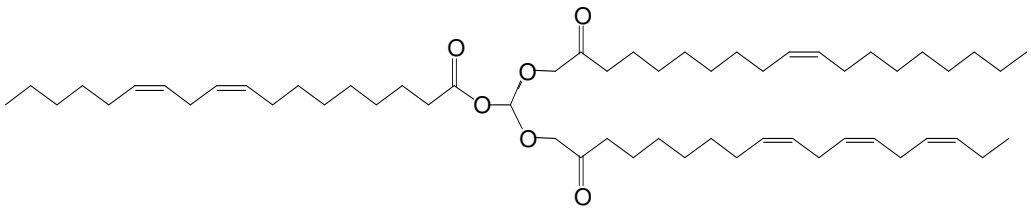

Figure 1-4 Triglyceride chain containing three fatty acid chains by a glycerol center.

Table 1-2 Many fatty acid contents in different oils [33].

Fatty acid	[#C: #DB*]	Canola oil	Corn oil	Linseed oil	Olive oil	Soybean oil	Tung oil	Fish oil
Palmitic	16:0	4.1	10.9	5.5	13.7	11.0	—	—
Stearic	18:0	1.8	2.0	3.5	2.5	4.0	4	—
Oleic	18:1	60.9	25.4	19.1	71.1	23.4	8	18.20
Linoleic	18:2	21.0	59.6	15.3	10.0	53.3	4	1.10
Linolenic	18:3	8.8	1.2	56.6	0.6	7.8	—	0.99
α-elaeostearic acid	—	—	—	—	—	—	84	—
Average #DB/triglyceride	—	3.9	4.5	6.6	2.8	4.6	7.5	3.6

*#C stands for number of carbon atoms in chain and #DB stands for the number of double bonds in that chain

1.4 Research objectives

The research goal for the first topic on MWCNT reinforced polymer composites is to develop carbon nanotube reinforced polymer composites by ROMP using two ROMP based monomers: DCPD and ENB. In order to overcome the issues of dispersion, load transfer, and interfacial interactions, the nanotube are functionalized by indirect covalent functionalization. After functionalizing the nanotubes, both DCPD and ENB ROMP-based composites with different nanotube loadings are fabricated. The influence of functionalized carbon nanotubes on the thermal and mechanical properties are evaluated and the difference between the composites from the two ROMP monomers is investigated.

The research goal for the second topic on biorenewable rubber is to develop bio-based elastomers. This effort is divided into two stages: synthesis of bio-renewable rubber and characterization of these polymer networks. The bio-rubber is synthesized using cationic polymerization. The characterization of rubber composites focuses on the thermal-mechanical properties of the elastomers, especially glass transition temperature and elongation, which should elucidate the possibility of the rubber for their potential use in tire or other applications, such as seals or rubber adhesive coatings.

1.5 References

[1] Ajayan PM, Stephan O, Colliex C, Trauth D. *Science* **265**, 1212, (1994).

[2] Web of Science, Search performed March 2009, Topic=(Polymer nanocomposite*), Timespan = 1994-2009, Databases=SCI-EXPANDED, SSCI, A&HCI, CPCI-S, CPCI-SSH.

[3] Baughman RH, Zakhidov AA, Heer WA. *Science* **297**, 787, (2002).

[4] Coleman JN, Khan U, Gun'ko YK. *Adv. Mater.* **18**, 1, (2006).

[5] Coleman JN, Khan U, Blau WJ, Gun'ko YK. *Carbon* **44**, 1624, (2006).

[6] Fu K, Huang W, Lin Y, Riddle LA, Carroll DL, Sun YP. *Nano Lett.* **1**, 439, (2001).

[7] Blake R, Gun'ko YK, Coleman J, Cadek M, Fonseca A, Nagy JB, Blau WJ. *J. Am. Chem. Soc.* **126**, 10226, (2004).

[8] Qin S, Qin D, Ford WT, Resasco DE, Herrera JE. *Macromolecules* **37**, 752 (2004).

[9] Hwang GL, Shieh Y-T, Hwang KC. *Adv. Funct. Mater.* **14**, 487, (2004).

[10] Buchmeiser MR. *Chem. Rev.* **100**, 1565, (2000).

[11] Rurstner A. *Angew. Chem. Int. Ed.* **39**, 3012, (2000).

[12] Novak BM, Risse W, Grubbs RH *Adv. Polym. Sci.* **102**, 47, (1992).

[13] Grubbs RH. Handbook of metathesis, vol. 3. Weinheim: Wiley-VCH; 2003.

[14] Buchmeiser MR, Sinner F, Mupa M, Wurst K. *Macromolecules* **33**, 32, (2000).

[15] Juang A, Scherman OA, Grubbs RH, Lewis NS. *Langmuir* **17**, 1321, (2001).

[16] Harada Y, Girolami GS, Nuzzo RG. *Langmuir* **19**, 5104, (2003).

[17] Watson KJ, Zhu J, Nguyen ST, Mirkin CA. *J. Am. Chem. Soc.* **121**, 462, (1999).

[18] Watson KJ, Zhu J, Nguyen ST, Mirkin CA. *Pure Appl. Chem.* **72**, 67, (2000).

[19] Weck M, Jackiw JJ, Rossi RR, Weiss PS, Grubbs RH. *J. Am. Chem. Soc.* **121**, 4088, (1999).

[20] In Encyclopedia of Chemical Technology, 4th ed.; Howe Grant, M., Ed.; Wiley-Interscience: New York, 1996; Vol. 17, 829

[21] Woodson CS, Grubbs RH. U.S. Patent 6020443, Advanced Polymer Technologies, Inc., 2000

[22] Li F, Hanson MV, Larock RC, *Polymer* **42**, 1567, (2001).

[23] Li F, Larock RC. *J Appl Polym Sci* **80**, 658, (2001).

[24] Li F, Larock RC. *J Polym Sci B Polym Phys* **38**, 2721, (2000).

[25] Li F, Larock RC. *J Polym Sci B Polym Phys* **39**, 60, (2001).

[26] Li F, Larock RC. *Polym Adv Technol* **13**, 436, (2002).

[27] Lehman SE, Wagnener KB. ADMET polymerization. In: Grubbs RH, editor. Handbook of metathesis. New York: Wiley-VCH; 2003. p. 283-353

[28] Calderon N. Olefin metathesis reaction. *Acc. Chem. Res.* **5**, 127, (1972).

[29] Tranka TM, Grubbs RH. *Acc. Chem. Res.* **34**, 18, (2001).

[30] Chen J, Hamon MA, Hu H, Chen Y, Rao AM, Eklund OP, Haddon RC. *Science* **282**, 95, (1998).

[31] Liu J, Rinzler AG, Dai H, Hafner JH, Bradley RK, Boul PJ, Lu A, Iverson T, Shelimov K, Huffman CB, Rodriguez-Macias F, Shon Y, Lee TR, Colbert DT, Smalley RE *Science* **280**, 1253, (1998).

[32] Tasis D, Tagmatarchis N, Bianco A, Prato M. *Chem. Rev.* **106**, 1105, (2006).

[33] Khot SN, Lascala JJ, Can E, Morye SS, Wiliams GI, Palmese GR. *J Appl Polym Sci* **82**, 703, (2001).

CHAPTER 2: TOUGHNESS ENHANCEMENT IN ROMP FUNCTIONALIZED CARBON NANOTUBE/POLYDICYCLOPENTADIENE COMPOSITES

A paper published in *Chemistry of Materials*[1]

Wonje Jeong[2], Michael R. Kessler[2,3]

2.1 Abstract

Norbornene functionalized multi-walled carbon nanotube (MWCNT)/dicyclopentadiene (DCPD) nanocomposites have been prepared by ring-opening metathesis polymerization (ROMP). Tensile toughness is shown to increase by over 900% compared to neat polyDCPD by incorporating just 0.4 wt% functionalized MWCNTs. Modest increases in modulus and strength were also observed with increasing nanotube loadings. The effect of norbornene grafted MWCNTs on the polymerization kinetics of the resulting cross-linked polyDCPD network was evaluated by differential scanning calorimetry (DSC). The glass transition temperatures of the composites are shown to increase with addition of functionalized MWCNTs. Moreover, decrease in damping behavior, as measured by dynamic mechanical analysis, is used to estimate the effective polymer-particle interphase thickness.

---

[1] Reprinted with permission of *Chemistry of Materials*,

[2]Graduate student and Assistant Professor, respectively, Department of Materials Science and Engineering, Iowa State University.

[3] Author for correspondence.

2.2 Introduction

Since the first report of polymer nanocomposites using carbon nanotubes (CNTs) as filler in an epoxy matrix in the mid 1990's [1], much interest has been shown by researchers within the polymer composites field. The high strength, modulus and large aspect ratios of CNTs combined with their unmatched electrical and thermal properties make nanotubes attractive candidates for multifunctional nano-reinforced polymer composites [2]. However their non-reactive surfaces and strong aggregative properties have limited the effectiveness of CNTs with the polymer matrices they reinforce. If the unique multifunctional properties of CNTs are to be utilized for effective reinforcement, well-dispersed nanotubes with good interfacial stress transfer with the polymer matrix is a prerequisite [3,4]. A number of surface-functionalization techniques have been proposed to tailor the nanotube surface for optimized compatibility with the polymer matrix. There are two main strategies for covalently functionalizing the nanotubes: the "grafting to" approach, which involves coupling of growing polymer molecules with reactive end groups to functional groups on the nanotube surface [5-7], and the "grafting from" approach, which propagates reactions from initiation sites or reactive groups covalently attached on the nanotube surface [8-11].

With the recent development of ruthenium based catalysts (Grubbs catalysts) which are tolerant of a wide range of polar functionalities, ring-opening metathesis polymerization (ROMP) has recently emerged as a powerful tool to synthesize well-defined macromolecular materials [12 - 18]. ROMP also has been developed for synthetic protocols for the modification of inorganic surfaces such as silica [19], silicon [20,21], and gold [22-25]; both "grafting from" and "grafting to" approaches are applied to polymerize to and from the surface.

ROMP is also important for the production of industrially applicable polymers, the most important being polydicyclopentadiene (polyDCPD). PolyDCPD is a crosslinked polymer with high modulus, excellent impact strength, and chemical resistance formed by ROMP of its bicyclic olefin monomer [26]. These features, along with its quality surface, low cost, and processability, are leading to widespread use of polyDCPD in high performance composite structures as a matrix material [27]. In order to use polyDCPD for a composite matrix the fillers need to be modified due to the highly nonpolar hydrophobic properties of DCPD. For example, Yoonessi *et al.* demonstrated that a high degree of nanoclay dispersion and partial exfoliation could be obtained using organically modified clay in a polyDCPD matrix processed through in situ ROMP [28,29].

Recently, we have developed self-healing materials which autonomically repair microcrack damage in structural composites [30-32]. In these systems, microencapsulated DCPD monomer and Grubbs catalyst are embedded within an epoxy matrix. When the material is damaged, the microcapsules rupture and release the DCPD healing agent into the damage region where the healing agent contacts the catalyst, polymerization is initiated, and the damage is repaired. These self-healing composites possess great potential for mitigating microcracks and hidden damage, enabling structures with longer lifetimes and less maintenance. However, in order for this potential to be realized, the mechanical and adhesive strength of the ROMP-based healing agent system must be improved. Herein, with an ultimate goal of developing ROMP-based nanocomposite healing agents, we evaluate the effect of low loadings (< 0.5 wt %) of CNTs on the mechanical properties of polyDCPD. High loadings of CNT reinforcements increase the viscosity of the liquid healing agents too dramatically, and are not considered in this work. The issue of dispersion, load transfer, and

interfacial interactions is addressed by incorporation of norbornene-functionalized multiwalled nanotubes (f-MWCNTs). We show that the use of f-MWCNTS leads to improved interfacial interactions and physical properties through covalent "tethers" between the nanotube reinforcement and the polymer network.

2.3 Experimental

2.3.1 Materials

The MWCNTs, produced by chemical vapor deposition (CVD) with O.D. × I.D. × length (15-20 nm × 5-10 nm × 0.5-200μm, > 95%) and dichloro(3-methyl-2-butenylidine)bis(tricclopentyl)phosphine ruthenium (Grubbs' catalyst 1st Generation) were purchased from Aldrich Co. PTFE membrane filters (Pall Corporation) with an average pore size of 400 nm were used for all filtering steps. *N,N'*,-Dimethylformamide (DMF), anhydrous ethylene glycol, and anhydrous pyridine were purchased from Aldrich and used without further purification. All other reagents and solvents were purchased from commercial suppliers and used as received. Both dicyclopentadiene (Alfa Aesar, 95+ %) and 5-norbornene-2-yl(ethyl)chlorodimethylsilane (Hybrid Plastics) were also used as received. To improve the dispersion and interfacial adhesion of carbon nanotubes we have developed a functionalization strategy where we first use acid treated MWCNTs to create –COOH functionalized nanotubes and then attached norbornene moities to the acid functionalized nanotubes as described below.

2.3.2 Synthesis of MWCNT-COOH

A two step procedure was used to prepare the MWCNT-COOH. First, as supplied MWCNTs (1.1g) and nitric acid (60%, 500 mL) were sonicated in an ultrasonic bath for 10

min to create an initial dispersion, followed by 6 hr reflux at 130 ^{o}C. The filtered product was rinsed with DI water until neutral pH. Since nitric acid reflux produces carboxyl, hydroxyl, and carbonyl groups at the defect sites of the MWCNTs, a second step of further oxidation with potassium permanganate solution in perchloric acid was performed to convert the hydroxyl and carbonyl groups to carboxyl groups using the procedure described by Sainsbury and Fitzmaurice [33] and by Kordas *et al.* [34]. The final solution was filtered again and dried under vacuum at 100 ^{o}C for 24 h, giving MWCNT-COOH (Figure 2-1(1)).

2.3.3 Synthesis of MWCNT-Norbornene

The MWCNT-COOH were refluxed in an excess of thionyl chloride with a catalytic amount of *N,N',*-Dimethylformamide (DMF) N_2 at 70°C for 48 h. The residual $SOCl_2$ was removed by high vacuum distillation, giving acyl chloride-functionalized MWCNTs (MWCNT-COCl) (Figure 2-1(2)) which was immediately reacted with 40 mL of ethylene glycol and 0.1 mL of pyridine at 120°C for 48 h, then purified. After cooling, the solution was filtered and repeatedly rinsed with THF and acetone. The product was dried under vacuum at 70 ^{o}C for 24 h, giving MWCNT-OH (Figure 2-1(3)). The MWCNT-OH was added in 5-norbornene-2-yl(ethyl)chlorodimethylsilane (25 mL) solution and 0.1 mL of pyridine and refluxed for 48 hr at 70 ^{o}C. The solution was filtered and washed fully with THF and dried under vacuum at 70 ^{o}C for 24 h, giving norbornene functionalized MWCNTs (Figure 2-1(4)).

2.3.4 Preparation of Nanocomposites

Norbornene functionalized MWCNTs (f-MWCNTs) were dispersed in DCPD by combining water bath and tip sonication. The crystal size and morphology of the Grubbs'

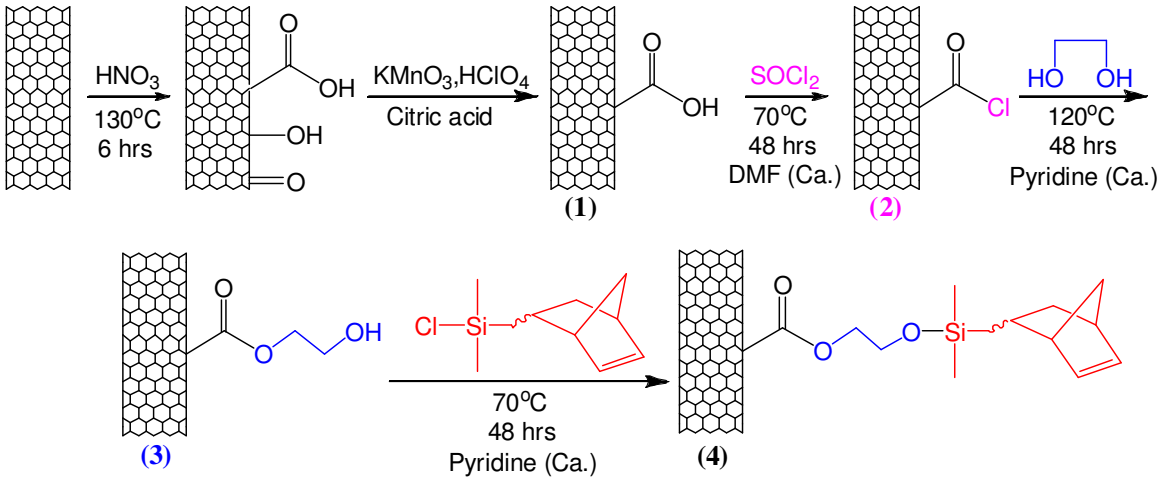

Figure 2-1. Schematic diagrams of functionalization of multiwall carbon nanotube.

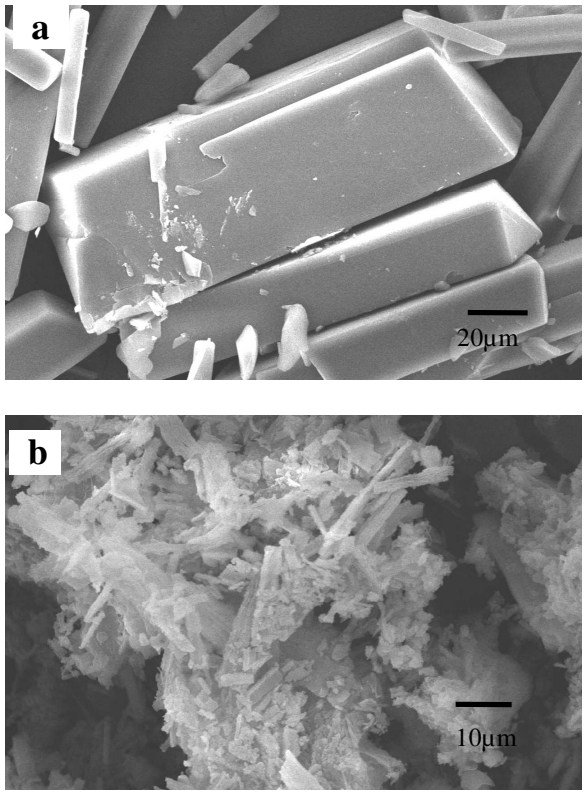

Figure 2-2. SEM of (a) as supplied Grubbs' catalyst from sigma-aldrich, (b) re-crystallized Grubbs' catalyst.

catalyst affects its dissolution kinetics in the monomer [35]. To recrystallize the catalyst into a more soluble form, it was first dissolved in dichloromethane (~20 x 10^{-3}g / mL) and subjected to dry nitrogen flow forming a much smaller catalyst crystal morphology than the 'as-received' catalyst (see Figure 2-2). The recrystallized catalyst was then mixed with the nanotube/DCPD solution (2.00 x 10^{-3}g of catalyst / 1 mL of DCPD) to dissolve the catalyst powder, forming a homogeneous solution, followed by curing for 2 hr at 70 ^{o}C and 1 hr 30 min at 170 ^{o}C. All mechanical tests were done one day after sample preparation to minimize the effect of surface oxidation [36]. The weight % was converted to volume fraction using equation 1.

$$V_f = \left[1 + \left(\frac{\rho_{NT}}{\rho_{pol}}\right)\left(\frac{1-m_f}{m_f}\right)\right]^{-1} \quad (1)$$

Where V_f and m_f are the volume fraction and weight fraction of the CNT filler respectively, and ρ_{NT} and ρ_{pol} are the density of CNTs and the polymer matrix respectively ($\rho_{NT}/\rho_{pol} = 2.2$) [37].

2.3.5 Characterization

Thermogravimetric analysis (TGA) was performed using a TA Instruments model Q50 TGA at a heating rate of 10 ^{o}C / min from room temperature to 850 ^{o}C with a continuous purge of air (40 mL/min). FTIR spectra were obtained from a Bruker Infared Spectrometer (IFS 66V/S). Samples were prepared as pellets using spectroscopic grade KBr. Differential scanning calorimetry (DSC) was analyzed using a TA Instruments model Q20 DSC. DCPD and f-MWCNTs/DCPD solutions (0.2 and 0.4 wt%) were mixed with recrystallized Grubbs' catalyst and quenched dropwise into liquid nitrogen to create small frozen droplets of catalyzed solution, preventing premature cure at room temperature. Finally, the small frozen

beads of catalyzed solution were placed into aluminum DSC sample pans and loaded into the DSC chamber at a standby temperature of -50 ^{o}C. The samples were scanned from -50 to 240 ^{o}C at a heating rate of 10 ^{o}C / min. Dynamic mechanical analysis (DMA) was investigated using a TA Instruments model Q800 DMA. Samples were analyzed in tension mode at 1.0 Hz over a temperature range of 30 to 210 ^{o}C at a heating rate of 3 ^{o}C / min. The sample dimensions were 35 × 5 × 1 mm. The glass transition temperatures (T_g) were determined from the peak temperatures of the tan δ curves. Tension tests were performed with a Universal Testing Machine (Instron 5569) equipped with a non-contact video-extensometer on ASTM D638 Type V samples at a crosshead speed of 1 mm/min. Each value reported is the average of at least four samples. The size distribution and dispersion status of f-MWCNTs in the matrix were obtained by transmission electron microscopy (JEOL 1200EX). Samples of acid treated and f-MWCNTs were prepared by evaporating drops of nanotubes dispersed in *N,N'*,-Dimethylformamide (DMF) solution on a carbon-coated copper grid. The composite was sliced into 70 nm thickness using an ultramicrotome for subsequent TEM analysis.

2.4 Results and discussion

It was not possible to create well dispersed suspensions of pristine nanotubes in DCPD monomer due to poor compatibility. As shown by optical microscopy (Figure 2-3a), when pristine MWCNTs/DCPD suspensions are removed from the sonication bath, the nanotubes remain separate from the DCPD and form several hundred micrometer scale aggregations. To obtain uniform distribution in the monomer, we introduced norbornene grafted MWCNTs using the procedures described above (see experimental methods), with

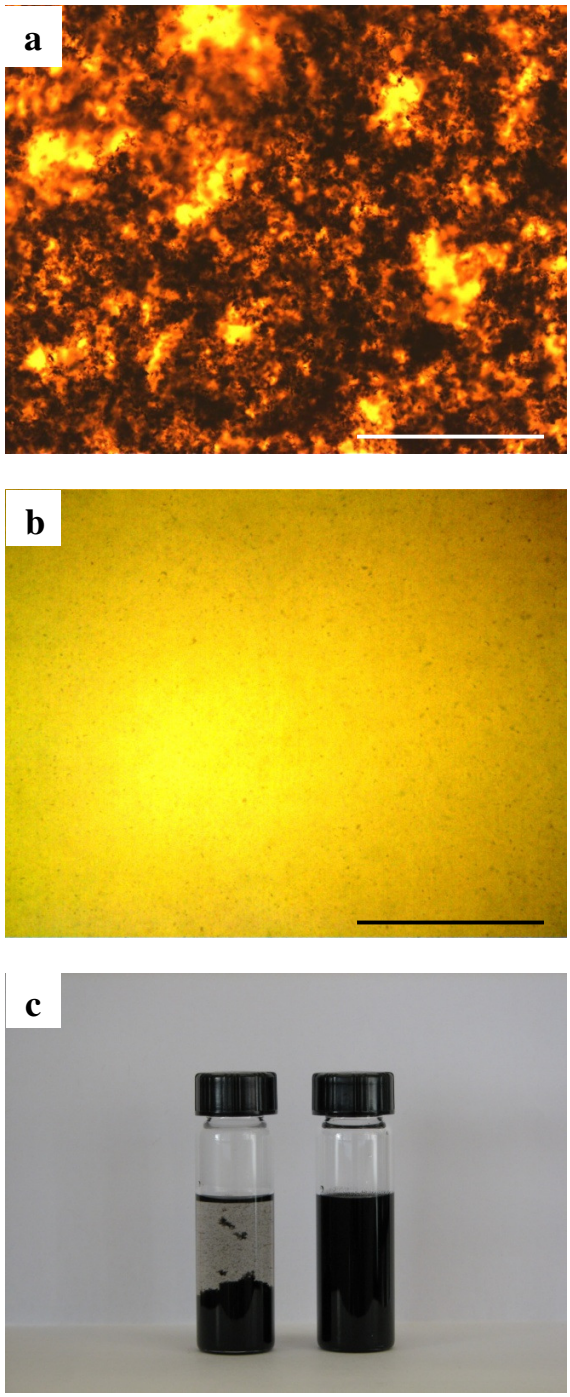

Figure 2-3. Optical microscopy images of the dispersion status of as supplied MWCNTs (a) and norbornene functionalized MWCNTs (b) in DCPD solution (0.5 mg/mL. scale bar = 1 mm), (c) Setting test of as supplied and functionalized nanotubes in DCPD monomer (Left: as supplied MWCNTs in DCPD monomer after 1 hr, Right: norborene functionalized MWCNTs in DCPD monomer after 1 day).

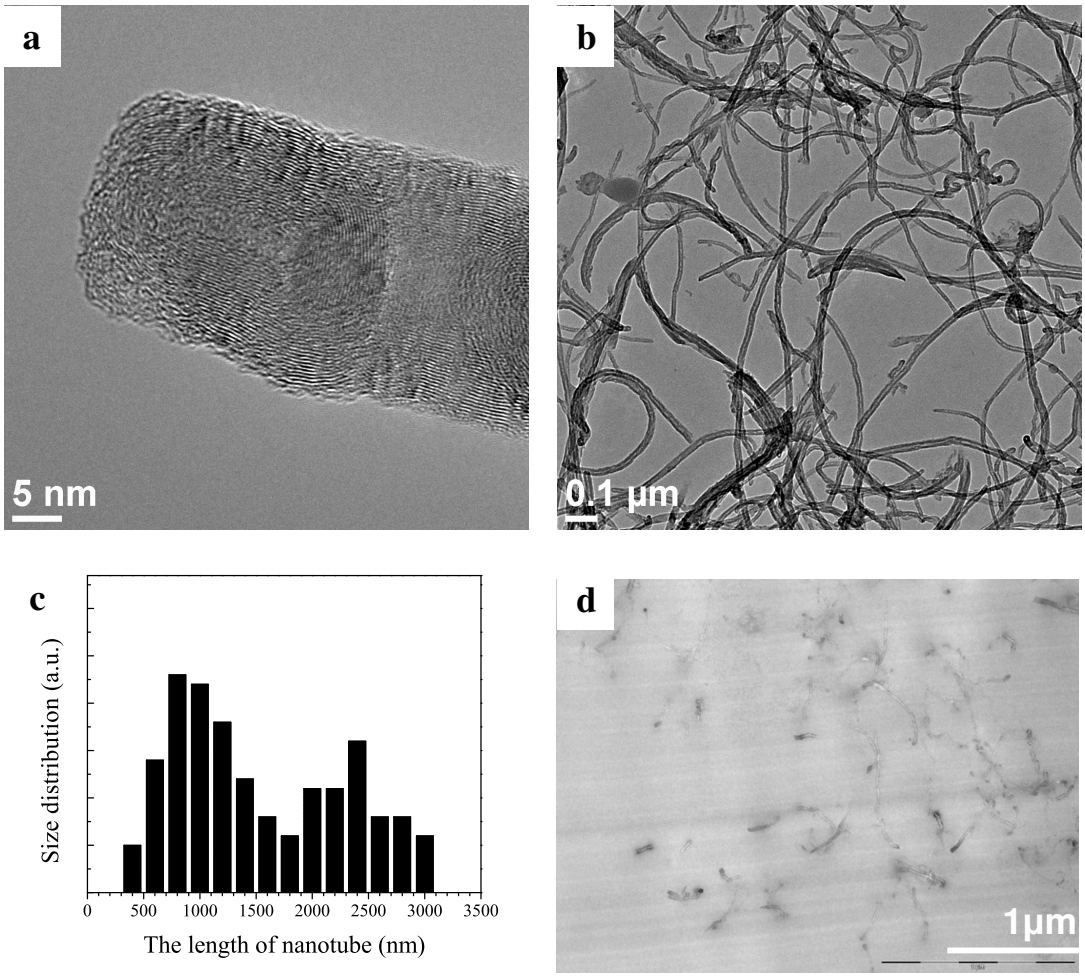

Figure 2-4. Transmission electron microscopy (TEM) images of (a) Acid treated MWCNT, (b) Norbornene functionalized MWCNT, (c) Size distribution plots of functionalized MWCNT, (d) Norbornene functionalized MWCNT/polyDCPD composites.

the expectation of improved compatibility between the nanotubes and the DCPD monomer. Optical microscopy shows that f-MWCNTs are well dispersed and homogeneously stable (Figure 2-3b). Figure 2-3c shows the dispersion of f-MWCNTs (right) compared to 'as supplied' MWCNTs (left) in DCPD monomer. The f-MWCNTs are dispersed in DCPD easily once sonication starts and remain stable indefinitely, whereas 'as supplied' MWCNTs agglomerate and settle to the bottom immediately following sonication. TEM images show that f-MWCNTs have a broad length distribution, from sub micrometer to 3 μm, which is shorter than expected, probably due to the harsh oxidation process and repeated sonication during functionalization (Figure 2-4).

Thermogravimetric analysis (TGA) was performed to verify the thermal stability of MWCNT (Figure 2-5a). The oxidized MWCNT-COOH decompose gradually with increasing temperature due to the decomposition of carboxyl groups on the surface of MWCNT-COOH and show a higher decomposition onset temperature compared to pristine MWCNTs due to the elimination of residue metal catalyst during acid treatment. The final weight for the 'as received' nanotubes is 7 wt%, corresponding to the residue metal catalyst used in CVD processing to form the nanotubes. For f-MWCNTs, there is significant weight loss between 250 – 400 ^{o}C (onset is at 292 ^{o}C) that may be attributed to the decomposition of the norbornene moieties. The reduction of decomposition temperature for the f-MWCNTs compared to MWCNT-COOH may be attributed to the stronger surface interaction between the carboxyl groups of the acid treated nanotubes which are much more closely packed together after drying in the vacuum oven. The increased weight loss may also be due to cleavage of weaker ether bonds or a retro Diels-Alder reaction possible in the f-MWCNTs. The quantity of the norbornene moiety functionalized to the surface of the nanotubes is

estimated from TGA as 16.85 wt% (at 480 ^{o}C). In the spectrum of acid treated nanotubes (Figure 2-5b top) the broad peak at 3100 ~ 3700 cm^{-1} is assigned to the O-H stretches of carboxyl groups. The peak at 1733 cm^{-1} corresponds to C=O stretch arising from the carboxylic acid groups. Figure 4b bottom shows the FTIR spectrum of f-MWCNTs. The peak at 1722 cm^{-1} is similarly assigned to the C=O stretch of the ester, while peaks at 1573, 1120, 1153 and 1440 cm^{-1} correspond to C=C bonds of norbornene, O-Si stretch, C-O stretch of the ester group, and C-H bend of alkyl chains respectively.

In order to make the MWCNT/DCPD nanocomposites, the f-MWCNTs/DCPD solution was mixed with recrystallized Grubbs' catalyst. Mixing DCPD with catalyst instantaneously initiates ROMP at room temperature. The catalyst opens the norbornyl double bond in DCPD, driven by ring strain relief, and a linear chain propagates. The remaining pentenyl double bond can be polymerized in a similar way to form a cross-linked polyDCPD network [38]. Two different types of polymerization mechanisms between f-MWCNTs and DCPD during ROMP are suggested. First propagating linear chains of DCPD encounter the norbornene moiety on the nanotube's surface and form covalent bonds in a "grafting to" approach (Scheme 2-6A). The other approach is that the norborne moiety on the nanotube surface can be initiated by Grubbs' catalyst resulting in catalyst-functionalized nanotubes, where the front Ruthenium catalyst subsequently reacts with surrounding DCPD to form the nanotube-polyDCPD network in a "grafting from" approach (Scheme 2-6B). Adronov *et al.* reported Grubbs' catalyst grafted single-walled carbon nanotubes using ROMP of norbornene and proposed that those functionalized catalysts on the surface of the nanotube can be used as rapid polymerization sites but bulk composites were not reported [39]. The second approach is kinetically favorable but statistically less likely due to the excess DCPD

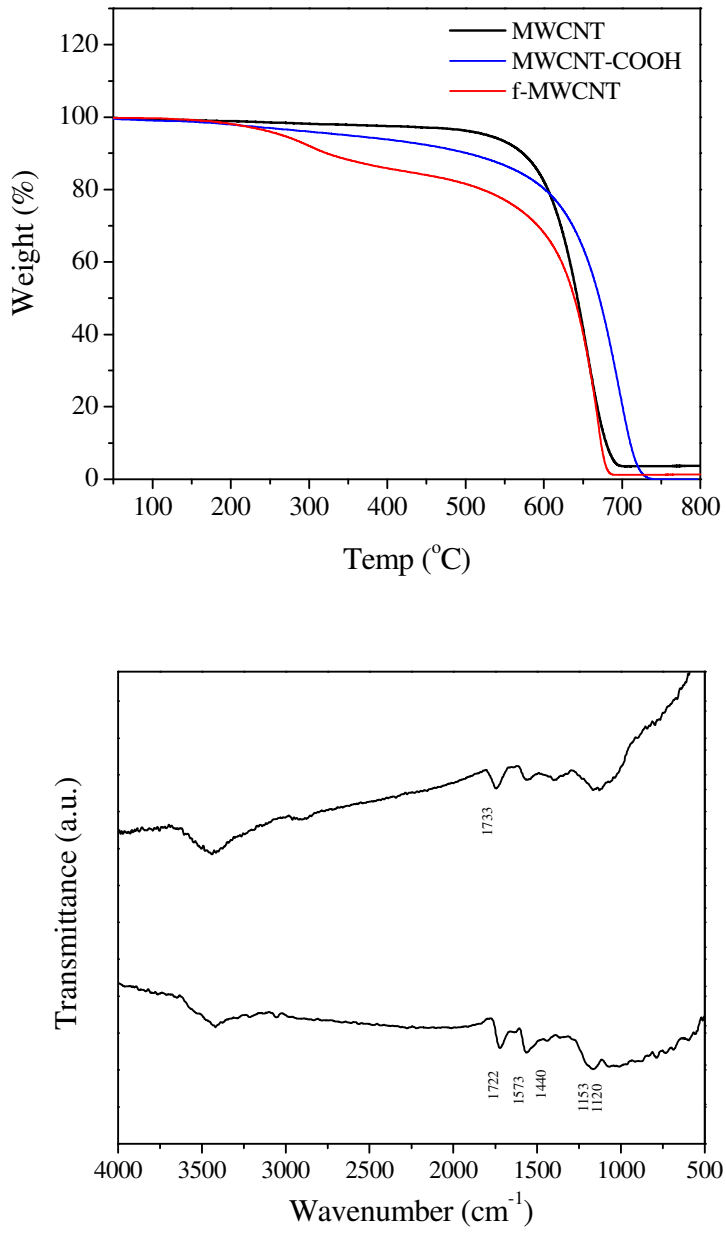

Figure 2-5. (a) Thermogravimetric analysis (TGA) weight loss curves of pristine, oxidized, and norbornene functionalized MWCNT (b) FTIR spectra of acid treated (top) and norbornene functionalized MWCNTs (bottom).

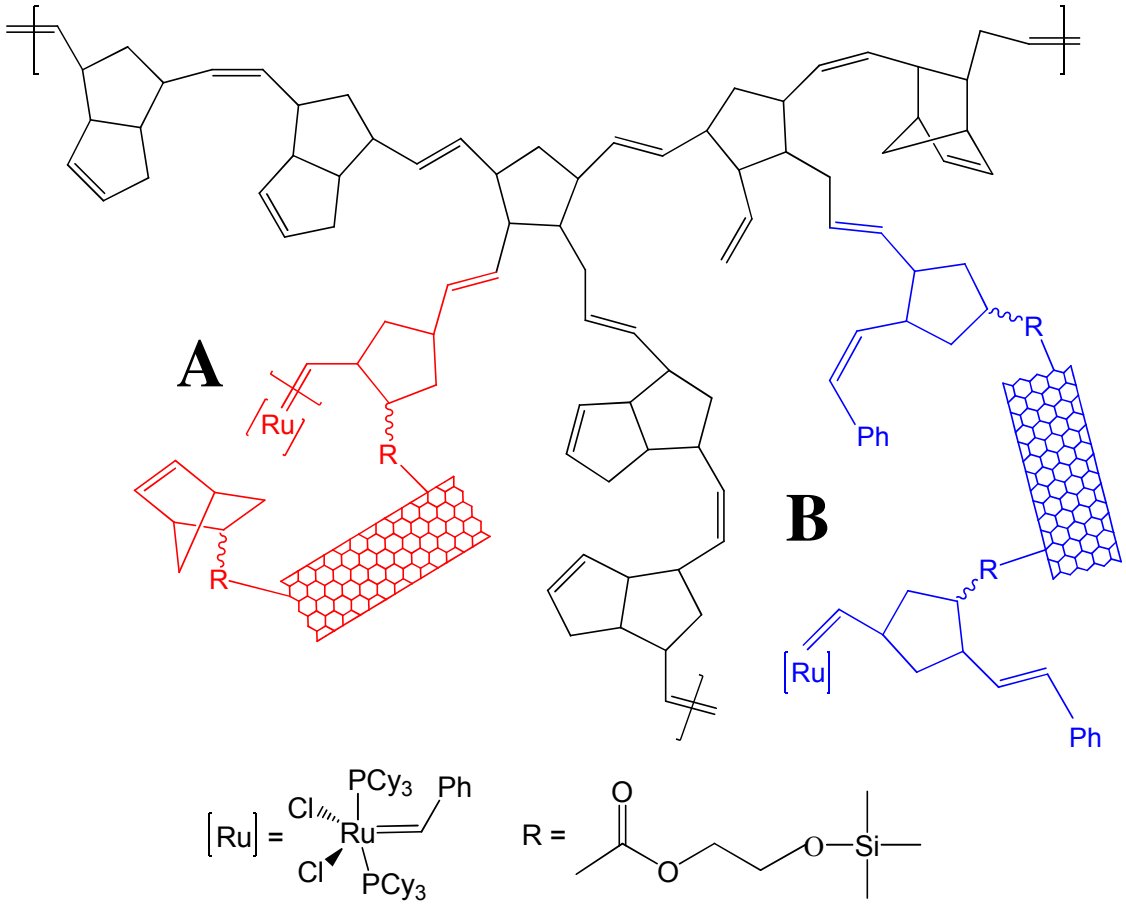

Figure 2-6. Schematic diagrams of polymerization mechanisms between norbornene functionalized MWCNT and polyDCPD by ROMP (A: grafting to, B: grafting from).

compared to f-MWCNTs. With the combination of these two different mechanisms, covalent bonds between f-MWCNTs and the polyDCPD are formed. These “tethers” between the nanotubes and the cross-linked network lead to improve interfacial stress transfer. Individual nanotubes are randomly dispersed throughout the matrix and no aggregation is observed by TEM observation of microtomed composite sections (Figure 2-4d). The scratched lines across the image in Figure 2-4d are due to microtome cutting.

Representative stress-strain curves for MWCNT/polyDCPD nanocomposites with different f-MWCNT loadings are shown in Figure 2-7. There is little increase of both Young’s modulus and strength for the composites with increasing CNT loading; however, noticeable increases of elongation at break are observed. Neat polyDCPD shows “typical” brittle thermoset tensile behavior. When the material is loaded to its ultimate tensile strength, the specimen fractures quickly at an elongation of 5.75% (Figure 2-8a). In contrast, with increasing nanotube loading, when the material reaches its ultimate tensile strength, yielding occurs, and the sample extends further. Macroscopic changes were observed in the tensile specimens during extension. Above the yield point, the reinforced samples neck, with a local decrease in width within the gauge region. The width of the neck region remains constant as its length increases so there is no further reduction in cross-sectional area and the necking zone propagates along the gauge region until the sample finally breaks (Figure 2-8b). The elongation at break significantly increased from 5.75 to 51.8 % with the addition of just 0.4 wt % f-MWCNTs. Figure 2-8c shows the tensile specimens following fracture, exhibiting the necking in the gauge region and the fracture phenomena. Upon incorporation of only 0.4 wt % nanotubes, the tensile toughness (from the total area under the stress strain curve) of the composites increased by 925 % in a linear fashion from 2.44 to 25 MPa (Figure 2-9). All

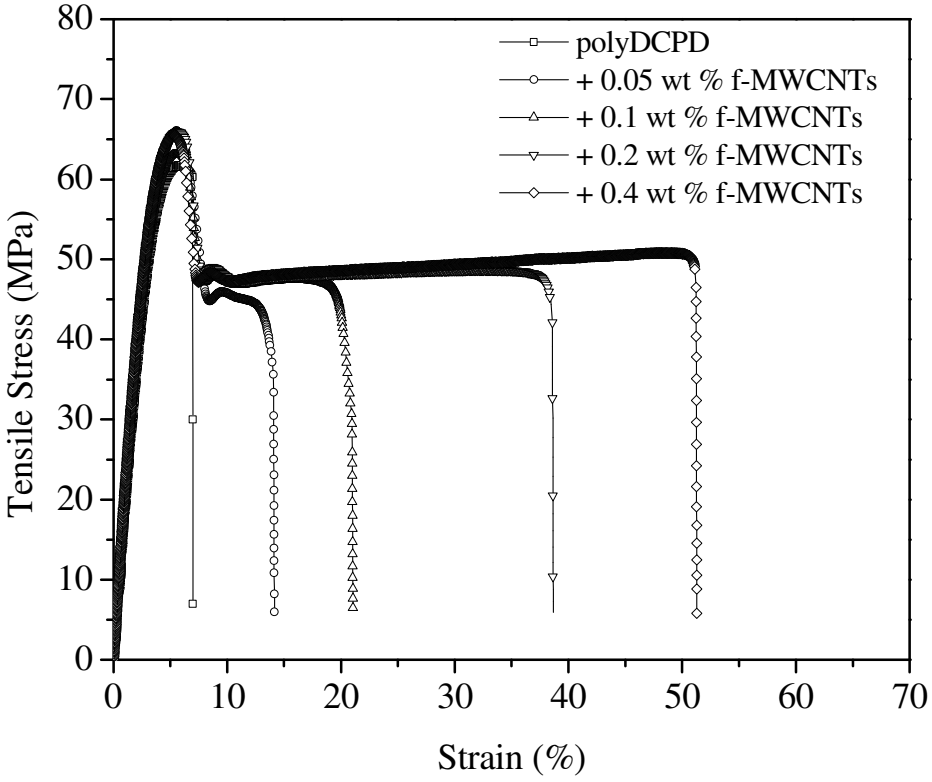

Figure 2-7. Representative stress-strain curves for norbornene functionalized MWCNT/polyDCPD composites with respect to nanotube weight percentage.

Table 2-1. Summary of Tensile test Results for f-MWCNT/polyDCPD Composite.

	E (GPa)	*E** (GPa)		σ (MPa)	ε_B (%)	Toughness (MPa)	Toughenss Change (%)
PolyDCPD	2.07 ± 0.026	2.07	2.07	62.9 ± 1.28	5.75 ± 0.06	2.44 ± 0.05	
+ 0.05 wt % f-MWCNTs	2.09 ± 0.015	2.09	2.07	63.9 ± 0.89	13.3 ± 4.36	6.31 ± 2.05	158.6
+ 0.1 wt % f-MWCNTs	2.11 ± 0.057	2.10	2.08	64.9 ± 1.23	19.5 ± 5.96	9.55 ± 3.46	291.4
+ 0.2 wt % f-MWCNTs	2.12 ± 0.073	2.14	2.08	65.1 ± 2.12	33.7 ± 4.41	16.1 ± 2.18	558.3
+ 0.4 wt % f-MWCNTs	2.14 ± 0.026	2.21	2.10	65.3 ± 1.03	51.8 ± 15.2	25.0 ± 7.27	925.9

*E** Young's modulus calculated by Halpin-Tsai equation

mechanical properties tested are tabulated in Table 1.

The increased elongation of f-MWCNT/polyDCPD nanocomposites could be due to several toughening mechanisms. First, carbon nanotubes have been shown to toughen composites by bridging crazes at the onset of matrix fracture [40]. Nanoparticles have also been known to increase fracture toughness through the formation of a large number of subcritical microcracks or microvoids and retard flaw coalescence into critical cracks [41], and to promote crack bridging effects and subsequent yielding of interparticle matrix ligaments [42,43]. Second, the interactions between the f-MWCNTs and polyDCPD (through covalent bonds) during ROMP (Figure 2-6) results in an interfacial region with properties and morphology which is different from the bulk polyDCPD network. Due to the large surface to volume ratio of the nano-reinforcement, this polymer specific interfacial region can become a dominant phase within the composite and vastly influence its thermo-mechanical behavior

As mentioned earlier there is little increase of modulus and strength due to the relatively low loading of f-MWCNTs. Normally in order to maximize load transfer from matrix to fillers, the length of fillers should be several times longer than a critical length**Error! Bookmark not defined.**, however nanotubes used in our experiment had broad length distributions with an average just below 2 μm (Figure 2-4c). The harsh oxidative process and repeated sonication during functionalization made the CVD-processed MWCNTs undesirably short. Worse is that many sub-micron length nanotubes are present, eliminating one of the key advantages of carbon nanotubes, high aspect ratio. The Halpin-Tsai model has been applied to predict the modulus of CNT-based polymer composites. There is a large variation in modulus for CVD-MWCNTs reported in the literature with

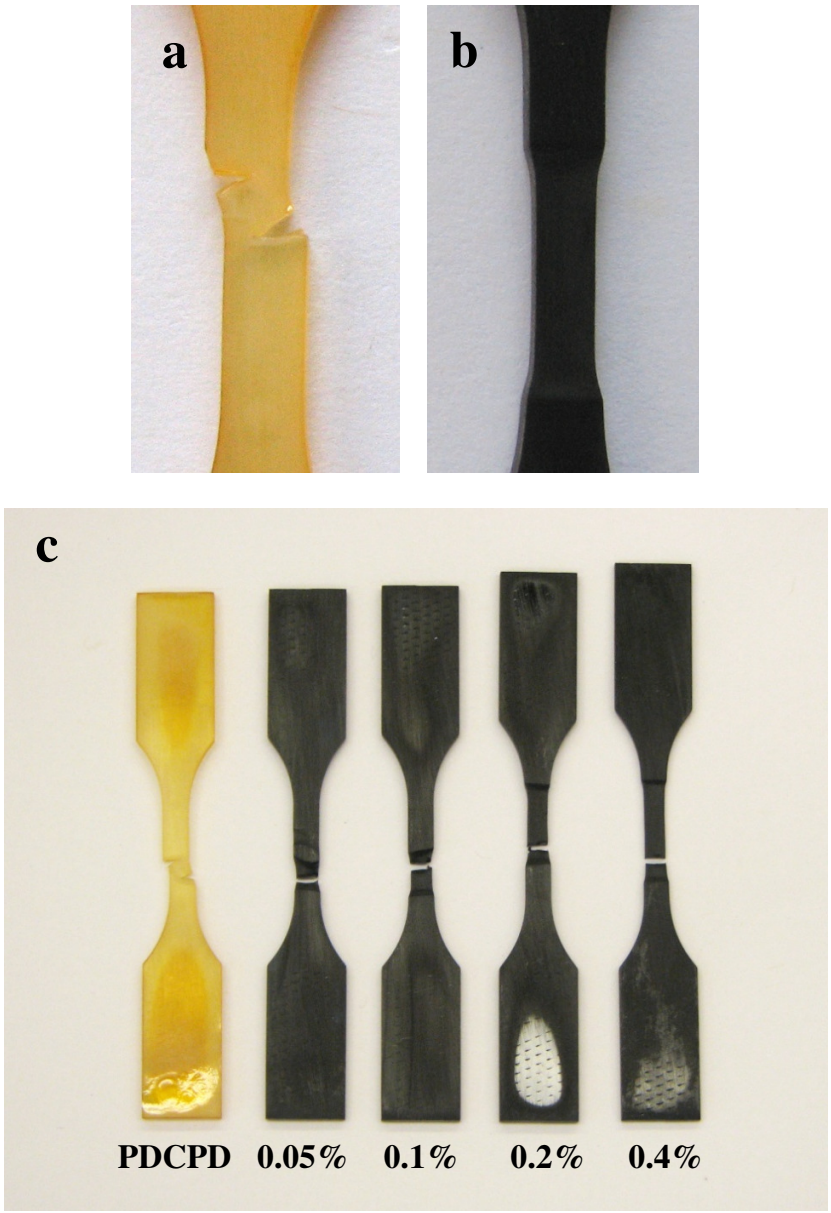

Figure 2-8. (a) Fractured morphology of brittle polyDCPD, (b) The reduction of gauge region during tension loadings of 0.4 wt % functionalized MWCNT/polyDCPD composite, (c) Morphological change of the length of elongated sample with gauge length and fractured shape.

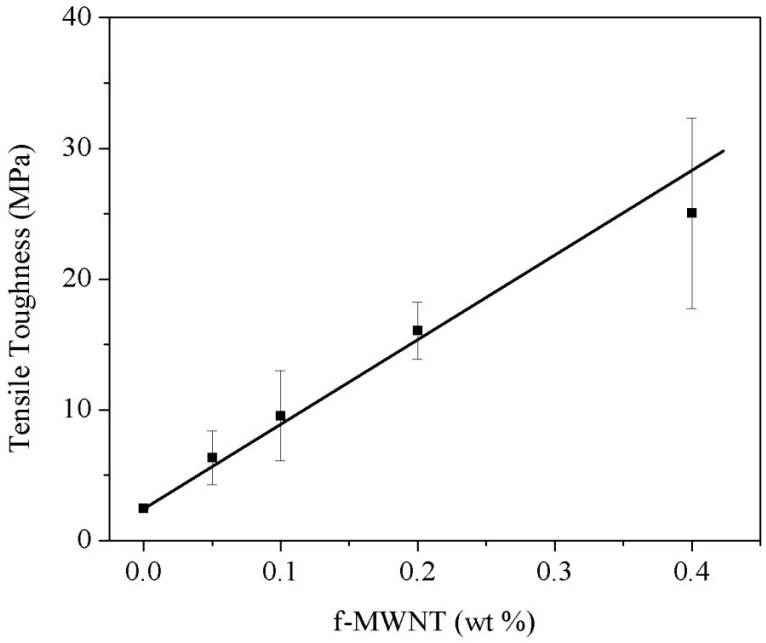

Figure 2-9. Changes of tensile toughness with respect to functionalized MWCNT loadings.

measured values ranging from 400 GPa [44] to just 50 GPa [45], which means that the modulus strongly depend on the concentration of defects. As such, the experimental values for composite stiffness are compared with Halpin-Tsai predictions using two different moduli of CVD-MWCNT: 400 GPa and 50 GPa. For randomly oriented CNTs in a polymer matrix, the modulus of the composite is given by following equation.

$$E_C = E_M \left[\frac{3}{8} \frac{1+2\left(l_{NT}/d_{NT}\right)\eta_L V_{NT}}{1-\eta_T V_{NT}} + \frac{5}{8} \frac{1+2\eta_T V_{NT}}{1-\eta_T V_{NT}} \right] \tag{2}$$

$$\eta_T = \frac{\left(\frac{E_{NT}}{E_M}\right)-1}{\left(\frac{E_{NT}}{E_M}\right)+2} \qquad \eta_L = \frac{\left(\frac{E_{NT}}{E_M}\right)-1}{\left(\frac{E_{NT}}{E_M}\right)+2\left(l_{NT}/d_{NT}\right)}$$

where E_C, E_{NT}, and E_M represent the tensile modulus of the composite, carbon nanotubes, and the polymer matrix, respectively; l_{NT} is the length of the nanotubes, d_{NT} is their diameter, and V_{NT} is the volume fraction of nanotubes in the composite. The estimated values are E_{NT} = 400 GPa for E^a and E_{NT} = 50 GPa for E^b, d_{NT} = 20 nm, and l_{NT} = 2 μm. The experimental data fall between the two calculated values and show good agreement within the volume fraction range explored (Table 1).

To investigate how the norbornene grafted nanotubes influence the curing kinetic of DCPD, dynamic DSC scans for the DCPD and two different wt % of f-MWCNTs with Grubbs' catalyst were performed (Figure 2-10). Dynamic scans shows a small endothermic peak near 18 ^{o}C from the melting of DCPD followed by a rapid exothermic peak corresponding to the ROMP of the DCPD monomer and the resulting relief of ring strain energy initiated by the highly reactive Grubbs' catalyst. It can be seen that there are distinct

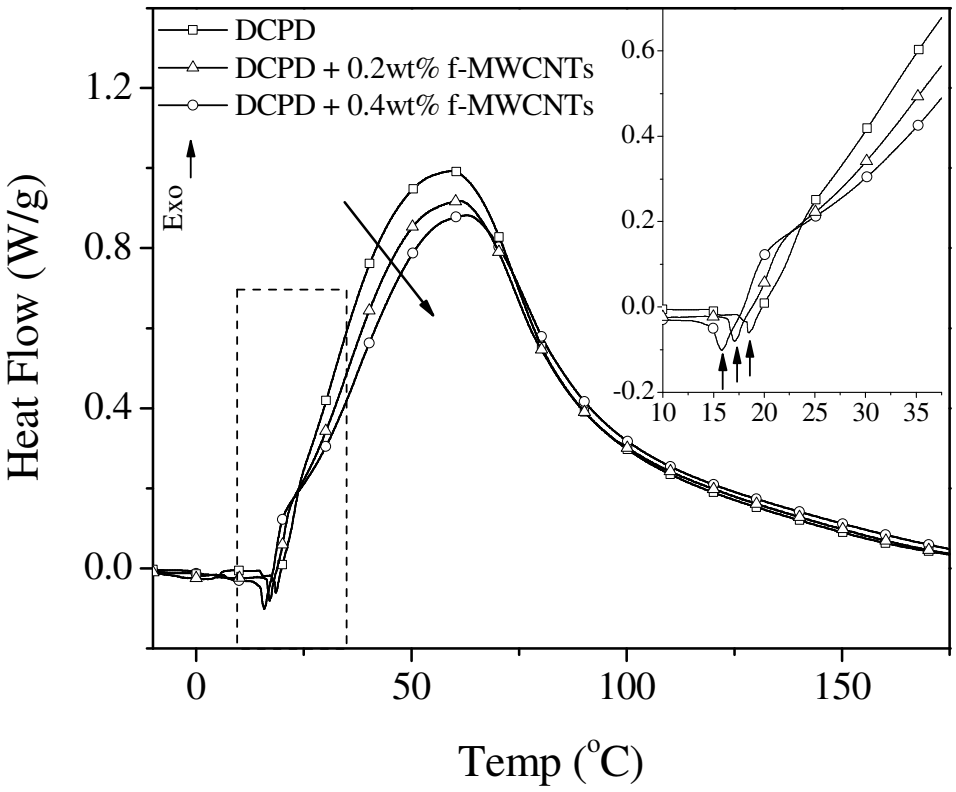

Figure 2-10. Differential Scanning Calorimetry dynamic scans at 10 °C / min.

differences between the neat DCPD monomer and the samples with added f-MWCNTs. For example, endothermic melting peaks gradually decrease from 18.5 to 15.8 ^{o}C with increasing nanotube loadings. Temperature scans of f-MWCNT/DCPD solution without Grubbs' catalyst (not shown) similarly exhibit decreasing melting points with increasing nanotube loading. The exothermic peaks shifted to higher temperature from 59.40 to 60.93 to 62.80 ^{o}C (for 0, 0.2, and 0.4 wt % respectively), indicating a slightly slower reaction rate with increasing nanotube loading. Furthermore the peak heights also decreased and the reaction heats gradually decreased from 375.5 to 371.7 to 368.0 J/g. However, the overall effect of f-MWCNTs on the cure behavior of the DCPD is relatively minor.

The thermal and viscoelastic properties of the nanocomposites have been investigated by DMA. The test was performed in order to evaluate the influence of norbornene f-MWCNT on the thermal and viscoelastic properties of the nanocomposites. Figure 2-11 shows the representative curves for storage modulus and tan delta as a function of temperature. As expected from tensile tests, the dynamic storage modulus only increases slightly in the glassy regions with increasing CNT loading. In general the glass transition temperature of nanocomposites depends on the interaction of nanofillers with the surrounding bulk polymer, increasing with attractive interactions (which yield wetted surfaces) and decreasing when effective free surfaces are formed [46,47]. In our sample, the addition of f-MWCNTs shows a gradual increase of T_g (except the 0.05 wt % f-MWCNT sample) and reduced damping of the composites. The T_g shifted from 153.85 ^{o}C to 159.15 ^{o}C for samples containing 0.4 wt % f-MWCNTs. The increase of thermostability may be interpreted as a reduction of the mobility of the polyDCPD around the nanotubes by covalent bonds between f-MWCNTs and the polyDCPD network. The magnitude of the tan delta

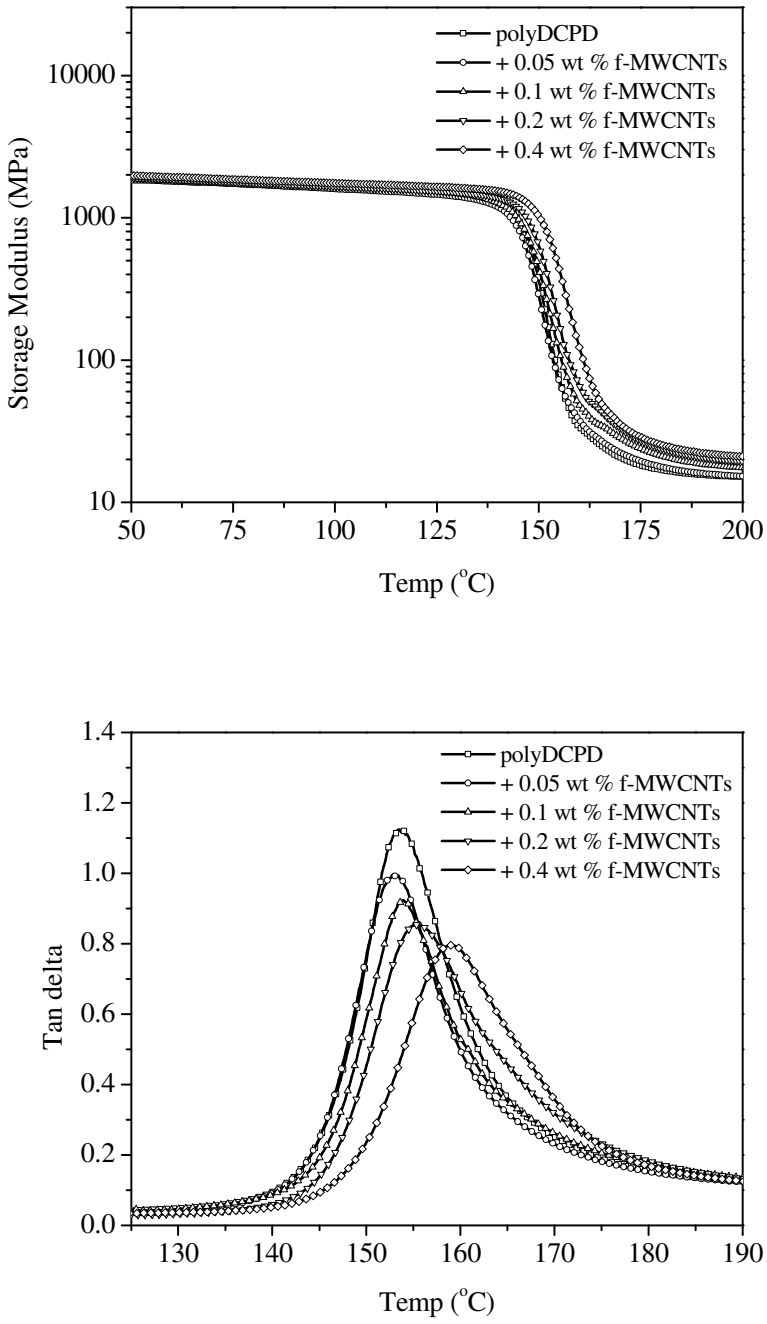

Figure 2-11. Dynamic mechanical analysis of functionalized MWCNT/poyDCPD composite: (a) storage modulus (*E'*) (b) tan δ.

Table 2-2. Summary of DMA Results for f-MWCNT/polyDCPD Composite.

	E' at (T_g +30 ^{o}C) (MPa)	T_g (tan δ) (^{o}C)	tan δ (peak height)	ΔR (nm)
PolyDCPD	16.3	153.9	1.12	
+ 0.05 wt % f-MWCNTs	18.8	152.9	0.99	226
+ 0.1 wt % f-MWCNTs	19.9	154.0	0.92	199
+ 0.2 wt % f-MWCNTs	22.0	155.5	0.85	164
+ 0.4 wt % f-MWCNTs	22.4	159.2	0.81	125

peak decreases with increasing f-MWCNT wt % (Figure 2-11b). If damping of the carbon nanotube is neglected (assuming perfectly elastic behavior) the effective interfacial thickness (ΔR) of the interphase between the CNTs and the polymer matrix can be estimated using the following equation [48,49].

$$\tan \delta_C = \tan \delta_m \left(1 - \left(1 + \frac{\Delta R}{R} \right)^2 V_f \right) \quad (3)$$

where, $\tan \delta_c$ is the damping of the composite, $\tan \delta_m$ is the damping of the matrix, V_f is the volume fraction of the functionalized nanotubes, and R is the radius of the anotubes. The calculated values are tabulated in Table 2. The effective interfacial thickness is about 200 nm at 0.05 wt % which is 10 times thicker than the diameter of the nanotube. There is a general decreasing function of ΔR with respect to volume fraction, presumably indicating that as volume fraction increases, there is a greater chance that there is overlap between the interfacial thickness of adjacent nanotubes. Additionally, we can assume that at lower volume fractions functionalized nanotubes are more ideally dispersed, and less likely to share interfacial volume.

2.5 Conclusions

Nanocomposites consisting of low loadings of norbornene functionalized MWCNTs and polyDCPD were developed. It was possible to achieve a homogeneous dispersion by grafting norbornene onto the nanotube surface. The investigation of mechanical properties of the nanocomposites resulted in a remarkable increase of tensile toughness (925 % increase over the neat polyDCPD) with just 0.4 wt % of functionalized MWCNTs. Cure kinetics of composites show that there are slight decreases of melting point, exothermic heat, and

reaction rate with increased nanotube loadings. DMA showed that there is a general increase of thermal stability (T_g) with the addition of functionalized nanotubes. Covalently bonded functionalized nanotubes reduce the mobility of the matrix by interfacial interactions resulting in a distinctive increase of glass transition temperature of the nanocomposites with nanotube loading. The dramatic effective interfacial thickness compared to the nanotube radius is additional evidence of strong interactions between the ROMP matrix and the nanotubes. Traditional methods for toughening thermosetting polymers with toughening agents typically come at the expense of other properties such as modulus, strength, or decreasing thermal stability. However, the system described here substantially increases the toughness, while at the same time increases the modulus and glass transition temperature using functionalized MWCNTs via ROMP.

2.6 Acknowledgment

The authors thank W. K. Geortzen, X. Sheng and T. C. Mauldin for their technical support and valuable discussions throughout the research and Prof. L. S. Chumbley for assistance in obtaining TEM images.

2.7 References

[1] Ajayan PM, Stephan O, Colliex C, Trauth D. *Science* **265**, 1212, (1994).

[2] Baughman RH, Zakhidov AA, Heer WA. *Science* **297**, 787, (2002).

[3] Coleman JN, Khan U, Gun'ko YK. *Adv. Mater.* **18**, 689, (2006).

[4] Coleman JN, Khan U, Blau WJ, Gun'ko YK. *Carbon* **44**, 1624, (2006).

[5] Fu K, Huang W, Lin Y, Riddle LA, Carroll DL, Sun YP. *Nano Lett.* **1**, 439, (2001).

[6] Lou X, Detrembleur C, Sciannamea V, Pagnoulle C, Jerome R. *Polymer* **45**, 6097, (2004).

[7] Blake R, Gun'ko YK, Coleman J, Cadek M, Fonseca A, Nagy JB, Blau WJ. *J. Am. Chem. Soc.* **126**, 10226, (2004).

[8] Qin S, Qin D, Ford WT, Resasco DE, Herrera JE. *Macromolecules* **37**, 752, (2004).

[9] Hwang GL, Shieh Y-T, Hwang KC. *Adv. Funct. Mater.* **14**, 487, (2004).

[10] Xia H, Wang Q, Qiu G. *Chem. Mater.* **15**, 3879, (2003).

[11] Tong X, Liu C, Cheng H-M, Zhao H, Yang F, Zhang X. *J. Appl. Polym. Sci.* **92**, 3697, (2004).

[12] Buchmeiser, MR. *Chem. Rev.* **100**, 1565, (2000).

[13] Rurstner A. *Angew. Chem. Int. Ed.* **39**, 3012, (2000).

[14] Calderon N. *J. Macromol. Sci. Rev. Macromol. Chem.* **7**, 105, (1972).

[15] Novak BM, Risse W, Grubbs RH. *Adv. Polym. Sci.* **102**, 47, (1992).

[16] Ivin KJ, Mol JC. Olefin metathesis and metathesis polymerization. San Diego: Academic Press; 1997.

[17] Frenzel U, Nuyken O. *J. Polym. Sci. Part A: Polym. Chem.* **40**, 2895, (2002).

[18] Grubbs RH. Handbook of metathesis, vol. 3. Weinheim: Wiley-VCH; 2003.

[19] Buchmeiser MR, Sinner F, Mupa M, Wurst K. *Macromolecules* **33**, 32, (2000).

[20] Juang A, Scherman OA, Grubbs RH, Lewis NS. *Langmuir* **17**, 1321, (2001).

[21] Harada Y, Girolami GS, Nuzzo RG. *Langmuir*, **19**, 5104, (2003).

[22] Watson KJ, Zhu J, Nguyen ST, Mirkin CA. *J. Am. Chem. Soc.* **121**, 462, (1999).

[23] Liu X, Guo S, Mirkin CA. *Angew. Chem.* **115**, 4933, (2003).

[24] Weck M, Jackiw JJ,q Rossi RR,Weiss PS, Grubbs RH. *J. Am. Chem. Soc.* **121**, 4088, (1999).

[25] Rutenberg IM, Scherman OA, Grubbs RH, Jiang W, Garfunkel E, Bao Z. *J. Am. Chem. Soc.* **126**, 4062, (2004).

[26] In Encyclopedia of Chemical Technology, 4th ed.; Howe Grant, M., Ed.; Wiley-Interscience: New York, 996; Vol. 17, 829.

[27] Woodson CS, Grubbs RH. U.S. Patent 6020443, Advanced Polymer Technologies, Inc., 2000.

[28] Yoonessi M, Toghiani H Kingery WL, Pittman CU. *Macromolecules* **37**, 2511, (2004).

[29] Yoonessi M, Toghiani H, Daulton, TL, Lin JS, Pittman CU. *Macromolecules* **38**, 818, (2005).

[30] White SR, Sottos NR, Geubelle PH, Moore JS, Kessler MR, Sriram SR, Brown EN, Viswanathan S. *Nature* **409**, 794, (2001).

[31] Kessler MR, Sottos NR, White SR. *Compos Part A-Appl S* **34**, 743, (2003).

[32] Liu X, Lee JK, Yoon SH, Kessler MR. *J Appl Polym Sci* **101**, 1266, (2006).

[33] Sainsbury T, Fitzmaurice D. *Chem. Mater.* **16**, 2174, (2004).

[34] Kordas K, Mustonen T, Toth G, Jantunen H, Lajunen M, Soldano C, Talapatra S, Kar S, Vajtai R, Ajayan PM. *Small* **2**, 1021, (2006).

[35] Jones AS, Rule JD, Moore JS, White SR, Sottos NR. *Chem. Mater.* **18**, 1312, (2006).

[36] Kelsey DR, Chuah HH, Ellison RH, Handlin DL, Scardino BM. *J. Polym. Sci. Part A: Polym. Chem.* **35**, 3049, (1997).

[37] Blond D, Barron V, Ruether M, Ryan KP, Nicolosi V, Blau WJ, Coleman JN. *Adv. Funct. Mater.* **16**, 1608, (2006).

[38] Fisher RA, Grubbs RH. *Makromol. Chem. Macromol. Symp.* **63**, 271, (1992).

[39] Liu Y, Adronov A. *Macromolecules* **37**, 4755, (2004).

[40] Qian D, Dickey EC, Andrews R, Rantell T. *Appl. Phys. Lett.* **76**, 2868, (2000).

[41] Wetzel B, Rosso P, Haupert F, Friedrich K. *Eng. Fract. Mech.* **73**, 2375, (2006).

[42] Cardwell BJ, Yee AF. *J. Mater. Sci.* **33**, 5473, (1998).

[43] Lee J, Yee AF *Polymer*. **42**, 589, (2001).

[44] Xie S, Li W, Pan Z, Chang B, Sun L. *J. Phys. Chem. Solids*. **61**, 1153, (2000).

[45] Salvetat JP, Kulik AJ, Bonard JM, Briggs AD, Stockli T, Metenier K, Bonnamy S, Beguin F, Burnham NA, Forro L. *Adv. Mater.* **11**, 161, (1999).

[46] Ash BJ, Schadler LS, Siegel RW. *Mater. Lett.* **55**, 83, (2002).

[47] Rittigstein P, Torkelson JM. *J. Polym. Sci. B* **44**, 2935, (2006).

[48] Vassileva E, Friedrich K. *J. Appl. Polym. Sci.* **89**, 3774, (2003).

[49] Iisaka K, Shibayama K. *J. Appl. Polym. Sci.* **22**, 3135, (1977).

CHAPTER 3: EFFECT OF FUNCTIONALIZED MWCNTS ON THE THERMO-MECHANICAL PROPERTIES OF POLY(5-ETHYLIDENE-2-NORBORNENE) COMPOSITES PRODUCED BY RING-OPENING METATHESIS POLYMERIZATION

A paper submitted to *Carbon*

Wonje Jeong[1] and Michael R. Kessler[1,2]

3.1 Abstract

Functionalized multiwalled carbon nanotubes (MWCNTs) reinforced poly(5-ethylidene-2-norbornene (ENB)) composites have been fabricated via ring-opening metathesis polymerization. Verification of covalent bond formation between the functionalized carbon nanotubes and the polyENB matrix was demonstrated by solvent exposure followed by thermal gravimetry. The tensile toughness of the composites increased by 300 % with dramatic morphological changes on the resulting fracture surfaces when just 0.8 wt % norbornene functionalized MWCNTs (f-MWCNTs) were added to the polymer. A slight increase of glass transition temperature was observed by dynamic mechanical analysis compared to a decreased value with unfunctionalized MWCNTs.

[1]Graduate student and Assistant Professor, respectively, Department of Materials Science and Engineering, Iowa State University.

[2] Author for correspondence.

3.2 Introduction

Much effort has been given to maximize the potential of nanoscale reinforcement in polymer nanocomposites during the last decade [1]. Despite this effort, the full potential of carbon nanotube reinforced polymers has not been realized because of difficulties in processing and limitations of load transfer between the matrix and nanotubes [2,3]. A commonly used strategy is modifying the surface of the reinforcement to increase interactions with the polymer matrix and to minimize the nano-reinforcement's self-attraction and aggregation. The covalent attachment of chemical functional groups to the surface of carbon nanotubes is one strategy to improve the efficiency of load transfer. In many cases the improvements in tensile strength and modulus are coupled with a reduction in strain at break, indicating a decrease in polymer toughness and flexibility, which is a common phenomenon in carbon nanotube reinforced polymer composites [4,5].

Recently we reported on the synthesis and characterization of polydicyclopentadiene (polyDCPD) thermoset materials reinforced with carbon nanotubes based on ring-opening metathesis polymerization (ROMP) [6]. The viability of ROMP nanocomposites has emerged due to recent developments by Grubbs and co-workers to develop ROMP catalysts which are tolerant of a wide range of functional groups [7]. ROMP provides a convenient and powerful tool for synthesizing functional polymers from ring-strained monomers such as norbornene and cyclooctene based monomers [8,9]. In the polyDCPD system, mechanical properties of the nanocomposites show a remarkable increase of tensile toughness (925 % increases over neat matrix) with addition of just 0.4 wt % functionalized multiwalled carbon nanotubes (f-MWCNTs) without sacrificing thermal stability. Our approach, which generated a direct covalent bond between the monomer, endo-dicyclopentadiene (DCPD), and the norbornene

terminated functional groups on the nanotube, used both a ‘grafting to’ and ‘grafting from’ concept via ROMP, and resulted in impressive increases of maximum elongation.

In this paper we investigate the ROMP based diene monomer, 5-ethylidene-2-norbornene (ENB), which can be polymerized by ROMP to produce a linear thermoplastic polymer. The difference between DCPD and ENB are the number of ROMP active double bonds and the curing kinetics, with the ENB being significantly more reactive than the endo-DCPD [10]. Using the same norbornene functionalized MWCNTs developed for our previous DCPD system [6], we investigate polyENB nanocomposites and the covalent interaction between the polymer matrix and the nanotube surface achieved by ROMP. In order to verify the effectiveness of the nanotube functionalization on the thermo-mechanical properties of polyENB, composites were fabricated with both functionalized and unfunctionalized “as-supplied” nanotubes. Fracture morphology and thermal stability of composites are also investigated.

3.3 Experimental

3.3.1 Materials

Two different types of carbon nantoubes were used in this work: “as-supplied” MWCNTs (as-MWCNTs) and norbornene-functionalized MWCNTs (f-MWCNTs). The as-MWCNTs, with O.D. × I.D. × length (15-20 nm × 5-10 nm × 0.5-200 μm), were purchased from Sigma Aldrich. In order to obtain uniform dispersion and strong interactions between the carbon nanotubes and the ENB monomer, norbornene functional groups were synthesized onto the nanotube surface. This synthetic functionalization procedure has been reported previously [6]; briefly as-MWCNTs are refluxed with nitric acid giving carboxylic acid

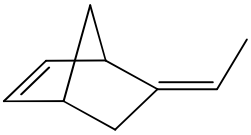

ENB

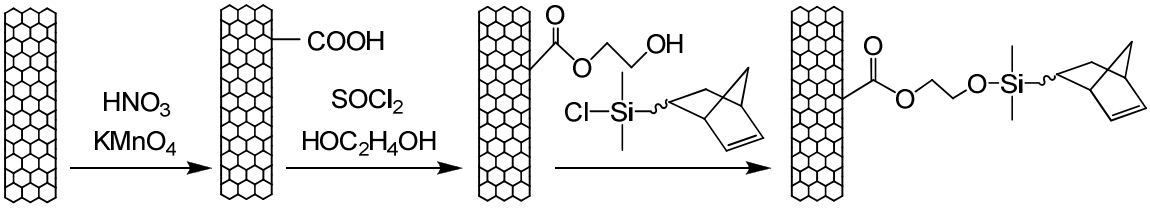

Figure 3-1 Chemical structure of ENB and schematic diagrams for functionalization of MWCNTs.

functionalized nanotubes (MWCNT-COOH). Consecutive reactions with thionyl chloride, ethylene glycol and 5-norbornene-2-yl(ethyl)chlorodimethylsilane gives norbornene f-MWCNTs. First generation Grubbs' catalyst (benzylidene-bis(tricyclohexylphosphine)dichlororuthenium) was used as a ROMP catalyst (Sigma Aldrich). The monomer, 5-ethylidene-2-norbornene (ENB, 99 %, Sigma Aldrich), was usedas received without further purification. The chemical structures of ENB and f-MWCNTs are shown in Figure 3-1.

3.3.2 Preparation of Nanocomposites

Both as-MWCNTs and norbornene f-MWCNTs were dispersed in ENB with a combination of sonication and shear mixing. For better dissolution kinetics of catalyst in ENB monomer, the catalyst was recrystallized from a dichloromethane solution (~20 mg/mL) to fine and soluble crystals by quickly evaporating the solvent with blowing nitrogen gas. The recrystallized catalyst was then mixed with the nanotube/ENB solution (0.4 mg of catalyst/1 mL of ENB) at - 40 ^{o}C using a 50:50 mixture of acetonitrile and dry ice bath. The cold bath was necessary to prevent the monomer from curing during mixing with Grubbs' catalyst, because ENB monomer has a very high reactivity at room temperature towards ROMP. The mixed samples were sequential cured for 30 min at 0 ^{o}C, 30 min at 25 ^{o}C, 2 h at 70 ^{o}C and 1 h 30 min at 170 ^{o}C.

3.3.3 Characterization

Solvent extraction and subsequent thermogravimetric analysis (TGA) was performed in order to quantify the amount of polyENB covalently bonded with f-MWCNTs during the ROMP processing of the composites. Neat polyENB is thoroughly dissolved in a boiling THF bath (boiling point of THF is 66 ^{o}C) within one hour. In contrast, a 1 g sample of 0.8

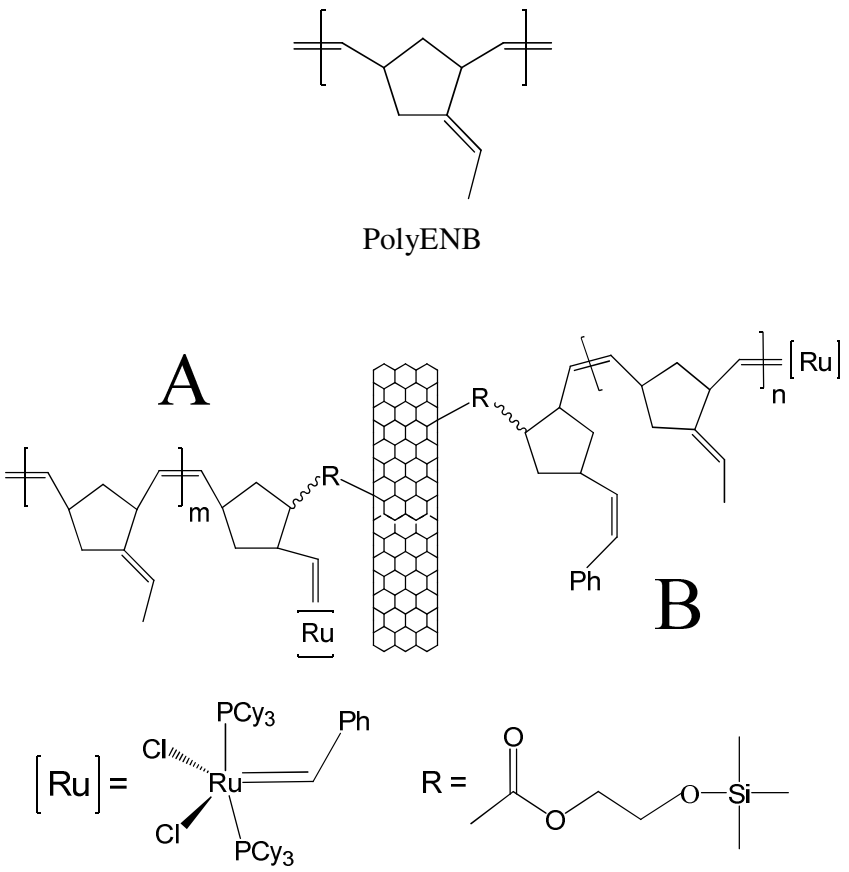

Figure 3-2 Two different types of polymerization mechanisms between f-MWCNTs and ENB during ROMP.

wt % f-MWCNT/polyENB was boiled for 24 hrs in a THF bath (500 mL) and filtered. The remaining black material was boiled again in a new THF bath for another 24 hrs to completely remove any uncrosslinked soluble polyENB from the nanotube surface. The solution was filtered again and a black sticky material was obtained. As a second step, the black material was soaked in THF at room temperature and washed at regular intervals for 7 days. The final black materials was dried and analyzed with a TGA (TA Instruments model Q50) at a heating rate of 10 ^{o}C /min under N_2 purge (40 mL/min).

Dynamic mechanical analysis (DMA) was performed using a TA Instrument model Q800 DMA. Samples were analyzed in tension mode at 1.0 Hz over a temperature range of 25 to 180 ^{o}C. The sample dimension was 33 × 5 × 1 mm. The peak temperature of the tan δ curve was used to determine the glass-transition temperatures (T_g) of the composites. Tension tests were performed with a Universal Testing Machine (Instron 5569) equipped with a non-contact video-extensometer on ASTM D638 Type V samples at a crosshead speed of 1 mm/min. Each value reported was the average of at least five samples. The fractured morphology of the samples was analyzed by scanning electron microscopy (SEM) using a Hitachi S-2460N variable pressure scanning electron microscope. The fracture surfaces were sputter coated under vacuum with gold prior to examination by SEM.

3.4 Results and discussion

The ROMP of ENB is a highly exothermic reaction due to the relief of ring strain energy, such that once polymerization starts, it generates significant heat which can accelerate the ROMP of ENB even at low temperature [10]. For this reason, the mixing and curing had to be performed at low temperature as mentioned in the experimental details

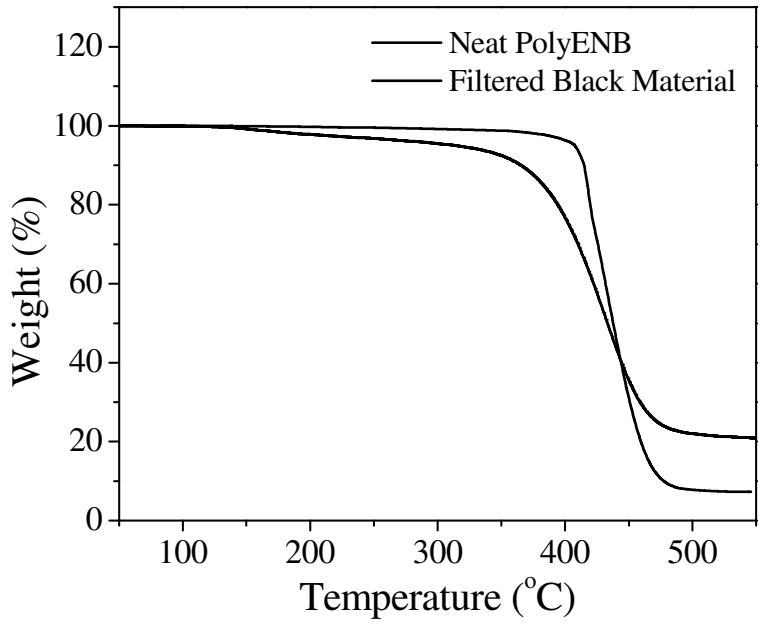

Figure 3-3 Weight loss curves for polyENB and filtered black material after solvent washing and drying of the composite. The filtered black material is hypothesized to be polyENB chemically bonded to functionalized carbon nanotubes.

above. During polymerization, the catalyst opens the norbornyl double bond in ENB, resulting in a linear polymer structure. Figure 3-2 suggests two possible polymerization mechanisms between f-MWCNTs and ENB during ROMP. The major mechanism can be considered a "grafting to" approach, where a rapidly propagating linear chain of ENB encounters the norbornene moiety on the nanotube's surface forming a covalent bond (Figure 3-2A). Considering the rapid polymerization rate of ENB monomer even at low temperature, it is less likely that a "grafting from" approach dominates, where the norbornene moiety on the nanotube surface is first initiated by Grubbs' catalyst resulting in chain growth from the nanotube surface (Figure 3-2B). However, both types of interactions may occur during ROMP between f-MWCNTs and ENB monomer. When the volume fraction of nanotubes is high the large interfacial region may also impact the rate of chain growth or chain termination.

In order to verify the assumed covalent attachment of polyENB onto f-MWCNTs and quantify the amount of bonded linear polymer chains with f-MWCNTs, the residual black material after solvent extraction (f-MWCNTs and covalently-linked polyENB chains prepared as described in the experimental section) was analyzed by TGA. The results are shown in Figure 3-3 for both the filtered black material and a polyENB control. The neat polyENB has a decomposition onset at 411 ^{o}C and just 7.36 wt % remaining residual material at 530 ^{o}C. The washed and filtered black material starts to lose mass slightly above 100 ^{o}C and rapidly begins to degrade at 350 ^{o}C, with a final residual mass of 21.14 wt % at 530 ^{o}C. Both samples show a maximum degradation rate (peak in -dw/dt) at approximately at 440 ^{o}C. On the basis of TGA results (knowing the residual mass of MWCNTs in N_2 up to 530 ^{o}C is over 90 %) the amount of polyENB chains covalently bonded to the f-MWCNTs can be

Table 3-1 Summary of tensile test results for two different types of nanotube/polyENB composites.

	E (MPa)	σ_y (Mpa)	ε_B (%)	Toughness (MPa)	Toughenss change (%)
PolyENB	1.89 ± 0.04	52.3 ± 0.6	29.4 ± 2.1	10.9 ± 0.8	
+ 0.4 wt % as-MWCNTs	1.96 ± 0.02	53.1 ± 0.1	22.9 ± 7.2	8.7 ± 2.8	- 20.6
+ 0.8 wt % as-MWCNTs	1.98 ± 0.04	53.2 ± 0.7	19.3 ± 4.4	7.5 ± 1.7	- 31.3
+ 0.4 wt % f-MWCNTs	1.97 ± 0.05	52.0 ± 1.1	18.0 ± 6.9	10.2 ± 1.1	- 6.4
+ 0.8 wt % f-MWCNTs	2.00 ± 0.04	52.0 ± 0.3	126 ± 6.3	46.3 ± 2.1	324.8
+ 1.6 wt % f-MWCNTs	2.02 ± 0.05	52.1 ± 0.2	105 ± 14	38.9 ± 5.4	256.9

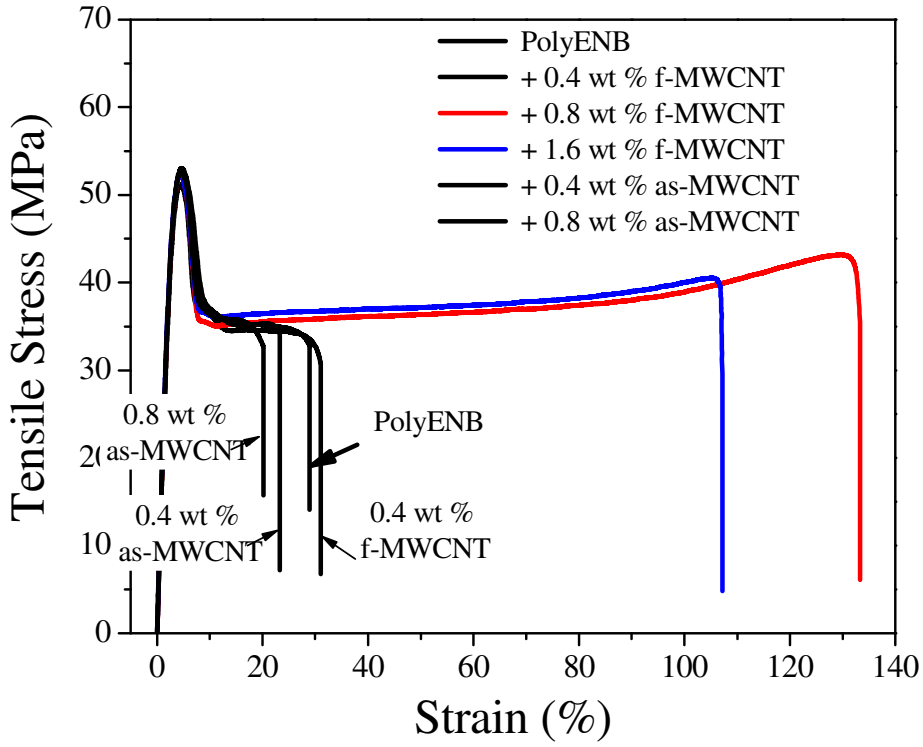

Figure 3-4 Representative stress-strain curves for as-supplied and norbornene functionalized MWCNT /polyENB composites with respect to nanotube weight percentage.

Figure 3-5 Morphological change of fractured gauge region after tension loadings of polyENB and 0.8 wt % functionalize MWCNT/polyENB composite.

calculated as roughly 80 %. These results give evidence of the existence of covalent bonds between the f-MWCNTs and the polyENB matrix via ROMP.

Representative stress-strain curves for MWCNT/polyENB nanocomposites with various weight percentages of carbon nanotubes are shown in Figure 3-4. Both as-MWCNTs and f-MWCNTs reinforced polyENB composites are developed to compare the effectiveness of functionalization on the mechanical properties of the composites. In all cases the composites show typical thermoplastic tensile behavior: the composite reaches its ultimate tensile strength where yielding occurs, followed by necking at 7 % elongation and then by a plateau region until fracture. The strain at fracture tends to decrease with increasing as-MWCNT content, dropping from 29% for neat polyENB to 19 % with 0.8 wt % as-MWCNTs. However there is significant increase of elongation up to 125 % at 0.8 wt % f-MWCNT loadings. Figure 3-5 shows a comparison of polyENB and 0.8 wt % f-MWCNT/polyENB specimens after the tension tests; the dog-bone specimens were the same length before testing. There is a dramatic morphological difference between the two pulled samples. Upon incorporation of 0.8 wt % f-MWCNTs, the tensile toughness (defined as the area under the stress strain curve) of the composite increased by 324 % (Table 3-1).

The increased elongation of f-MWCNT/polyENB nanocomposites may be due to interactions between the f-MWCNT and polyENB matrix during ROMP (Figure 3-2). Those interactions result in an interfacial region with properties and morphology that is different from the bulk polyENB properties. Since the nanotubes have such a large surface to volume ratio this interfacial region can become a dominant phase within the composite. In ideal cases, where a combination of perfect dispersion and interfacial interactions exist, as the nanotube weight percentage increases, modulus, strength, toughness, and fracture strain are

all expected to increase. In general, however, there is an optimum loading of reinforcement in polymer nanocomposite systems for maximum property enhancement. Because of dispersion and processing issues at large nanotube loadings, adding too much reinforcement can be counter-productive. In our system, 0.8 wt % of f-MWCNTs maximized the strain to failure and toughness; however, there were not huge improvements of Young's modulus compared to the significant increases in elongation.

The Halpin-Tsai model has been used to calculate the modulus of randomly oriented CNT reinforced polymer nanocomposites [11-14]. The details of the Halpin-Tsai equation and the length distributions of MWCNTs needed for the model are described in detail in our previous work [6]. A wide range of values for the modulus of MWCNTs have been reported in the literature, possibly because of variations in defect density in the nanotubes [15,16]. For this reason, we used three different modulus values of MWCNTs in the Halpin-Tsai equation for comparison: 50 GPa, 200 GPa, and 400 GPa. It can be seen from Figure 3-6 that the moduli for composites with different f-MWCNT loadings lie between the calculated values. The experimental data for composites with 0.17 Vol. % (0.4 wt %) f-MWCNTs fits well with the calculated Young's modulus of the composite if E_{NT} = 200 GPa. However, the increase in modulus with nanotube loading is not linear, and the Halpin-Tsai equation at E_{NT} = 200 GPa over-predicts the composite modulus at higher nanotube loading levels.

Figure 3-7a, and 3-7b show low magnification SEM images of tensile specimen fracture surfaces from composites containing 0.8 wt % as-MWCNTs and f-MWCNTs respectively. It is clear that large clusters of as-MWCNTs can be found on the fracture surface. A closer look in Figure 3-7c illustrates that aggregate blocks of the chemical vapor deposition (CVD) grown as-MWCNTs are present in the matrix. The CVD block shown here looks nearly

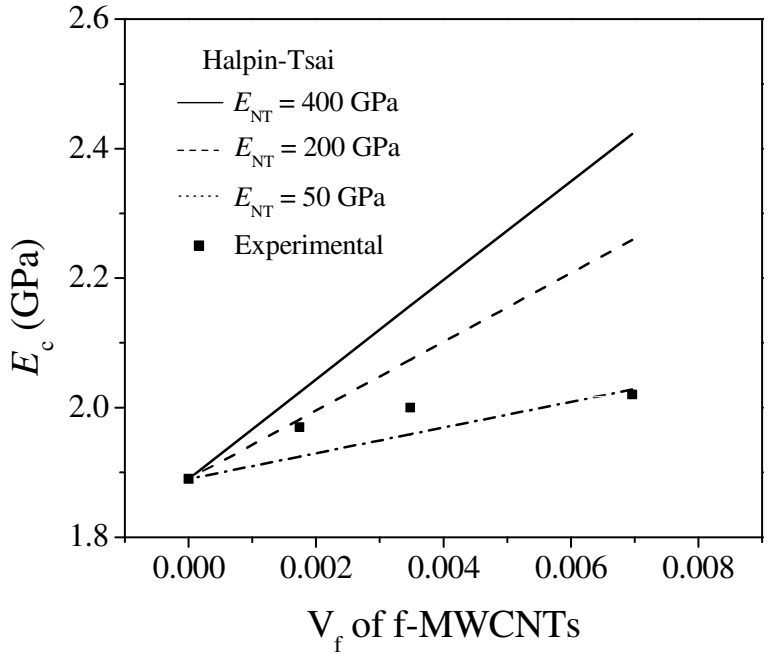

Figure 3-6 Theoretical Halpin-Tsai models and experimental data for the f-MWCNT/polyENB composites at various nanotube loadings.

Identical to unprocessed as-MWCNTs (before mixing with the resin) shown in the small picture in the bottom of Figure 3-7c. This indicates that ENB monomer has such poor compatibility with the nanotubes that even the combination of sonication and high shear mixing does not adequately disperse the nanotubes in the ENB matrix. The as-MWCNT/polyENB fracture surface is rough and jagged with aggregated as-MWCNT block cluster assumed to be the origin of fracture. The f-MWCNT/polyENB fracture surface is smoother and absent of obvious nanotube clusters. Figure 3-5d shows a high resolution SEM of the same fracture surface and indicates that the f-MWCNTs are dispersed individually. The f-MWCNT/polyENB samples have much smaller fracture surface areas than the as-MWCNT samples due to necking (Figure 3-7).

The thermal and viscoelastic properties of the nanocomposites have been investigated by DMA. These tests were performed in order to evaluate the influence of the carbon nanotube functionalization on the thermal and viscoelastic properties of the composite. Figure 3-8 shows representative curves for storage modulus and tan delta as a function of temperature. In general, the glass-transition temperature of the nanocomposites depends on the interaction of reinforcement with the matrix, increasing with stronger interfacial interactions [17,18]. The glass-transition temperature (measured as the peak in the tan δ curve) of as-MWCNT reinforced samples results in a decreased T_g by 4 ^oC with 0.8 wt % as-MWCNT. This decrease in T_g indicates that the poorly dispersed nanotubes with weak polymer interfacial interaction disrupt the polyENB network, reducing thermal stability. In f-MWCNT samples, the addition of f-MWCNT results in a slight increase of T_g (increasing 1.5 ^oC at 1.6 wt % f-MWCNT). This result suggests that the mobility of polyENB linear chains is hindered by chemical bonds with f-MWCNT. Both composites show decreasing damping

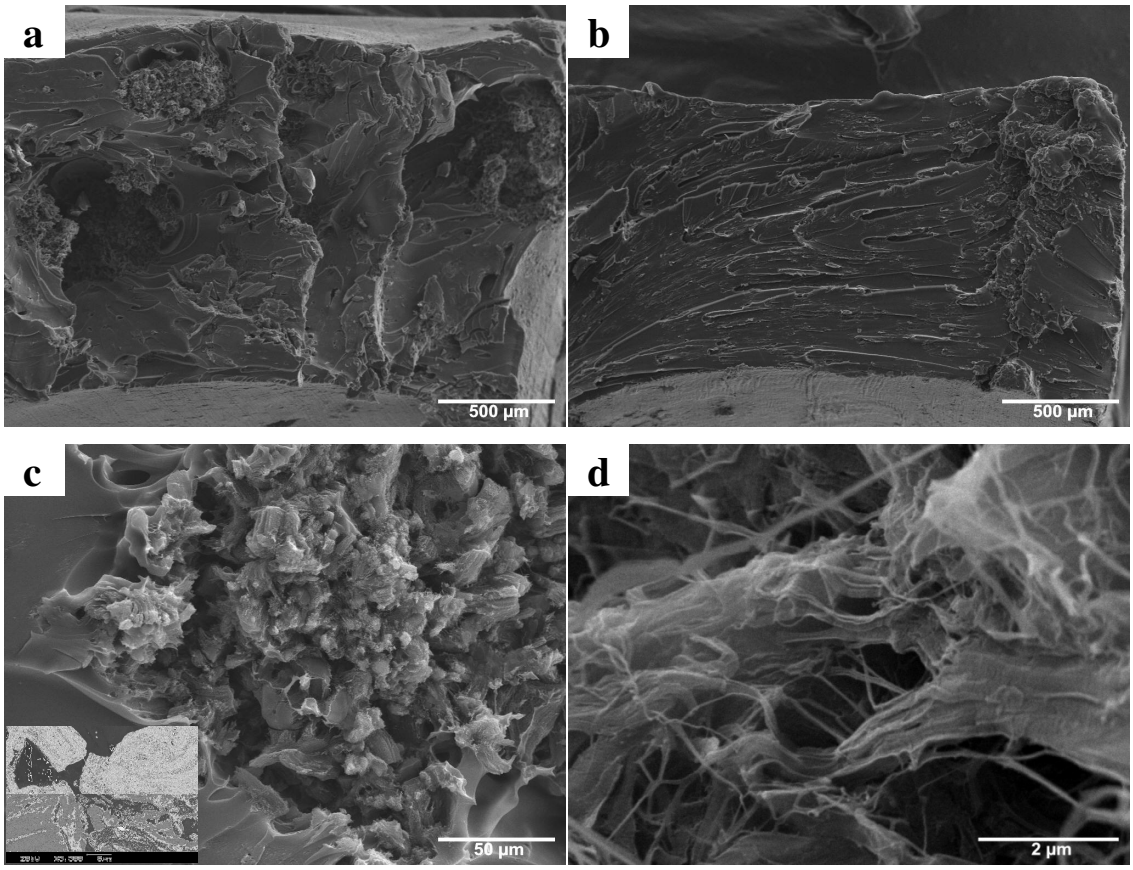

Figure 3-7 SEM image showing fracture morphology of failure surface for polyENB composites containing (a) 0.8 wt % as-MWCNTs and (b) 0.8 wt % f-MWCNTs; (c) and (d) are enlarged micrographs of (a) and (b) respectively. The insert in (C) is an image of the as-MWCNTs before processing in the composite.

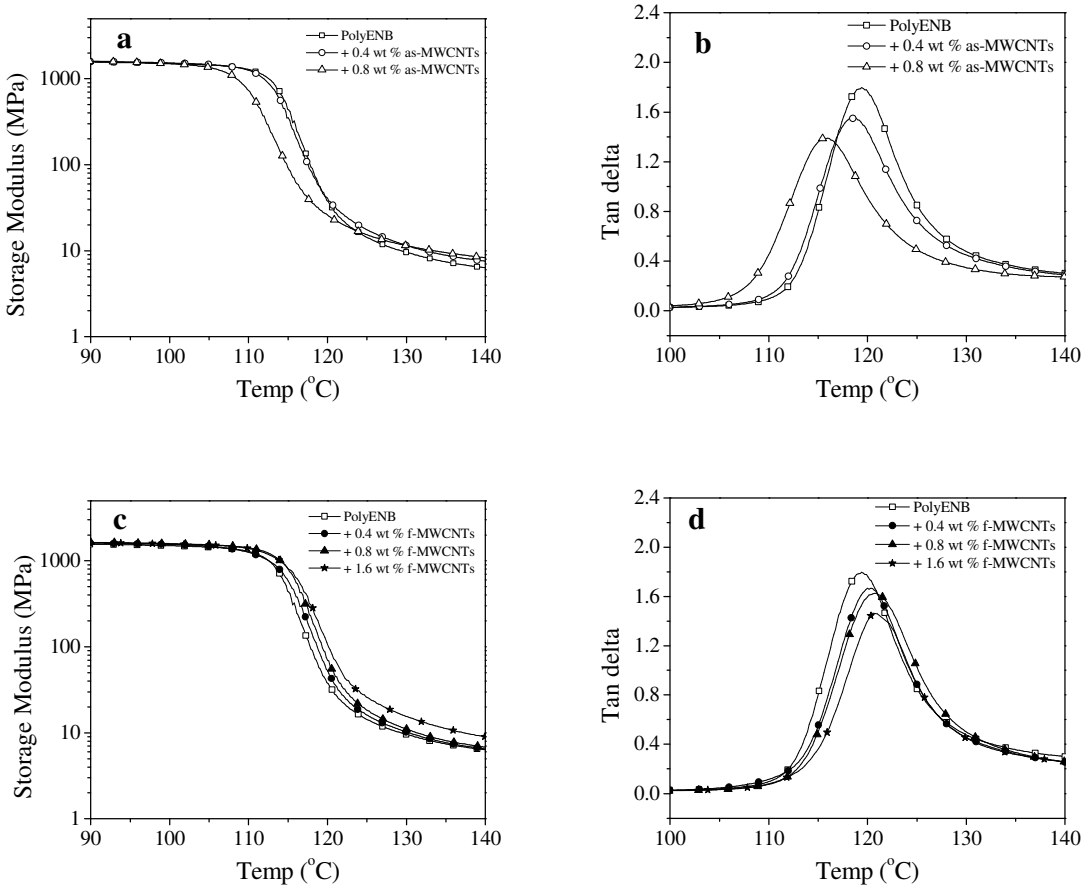

Figure 3-8 Dynamic mechanical analysis of composites: (a) storage modulus (*E'*) of as-MWCNT system (b) tan δ of as-MWCNT system (c) storage modulus (*E'*) of f-MWCNT system (d) tan δ of f-MWCNT system.

Table 3-2 Summary of DMA results for polyENB composite.

	E' at (T_g +30 ^{o}C) (MPa)	T_g (tan δ) (^{o}C)	tan δ (peak height)
PolyENB	5.3	119.4	1.8
+ 0.4 wt % as-MWCNTs	6.2	118.9	1.6
+ 0.8 wt % as-MWCNTs	6.7	115.9	1.4
+ 0.4 wt % f-MWCNTs	5.4	120.3	1.7
+ 0.8 wt % f-MWCNTs	5.5	120.7	1.6
+ 1.6 wt % f-MWCNTs	6.2	121.0	1.5

properties with nanotube loadings, which is expected for nanotube samples because of the incorporation of completely elastic (tan δ ~ 0) nanotubes in the polymer matrix. All experimental thermo-mechanical data are tabulated in Table 3-2.

The thermal decomposition behavior and the derivative TGA curves of polyENB and f-MWCNT/polyENB composites are shown in Figure 3-9. The TGA experiments demonstrate that the onset of thermal decomposition temperature gradually decreased from 411.4 (for neat polyENB) to 401.7 ^{o}C (for 1.6 wt% f-MWCNT/polyENB) with increasing f-MWCNT loadings. While the decomposition onset decreases with nanotube loadings, the maximum rate of decomposition remains about the same (at ~ 430 ^{o}C). The amount of residue remaining at 530 ^{o}C increased from 7.36 % (for neat polyENB) to 9.12 (for 0.8 wt % f-MWCNT/polyENB) to 10.15 % (for 1.6 wt % f-MWCNT/polyENB).

3.5 Conclusions

In summary, norbornene f-MWCNT reinforced polyENB nanocomposites were developed using ring-opening metathesis polymerization. The covalent linkage between norbornene moieties on the nanotube surface with the polymer matrix, as demonstrated by TGA, provides improved compatibility and subsequent higher elongation of the polyENB matrix. A significant enhancement of the toughness of polyENB nanocomposites is obtained at nanotube loadings of 0.8 wt %. The huge increased elongation indicates that the ROMP approach for surface interactions between nanotube and polymer matrix is very effective. The slight increase in glass transition temperature, as measured by DMA, for the f-MWCNT composites indicates a strong polymer interfacial interaction in these systems compared to composites with as-MWCNTs (which showed a slight decrease in T_g with nanotube loading).

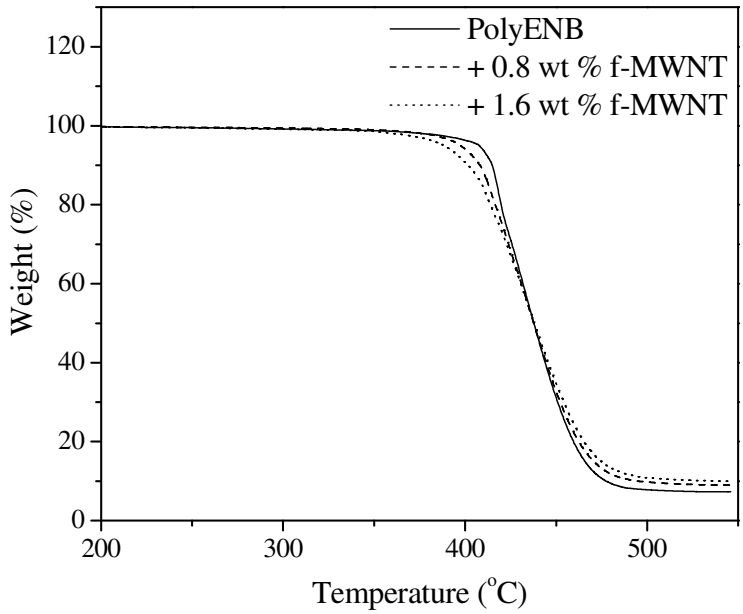

Figure 3-9 Thermogravimetric analysis of polyENB and composites with 0.8 and 1.6 wt% f-MWCNTs.

3.6 Acknowledgement

The authors thank X. Sheng and T. C. Mauldin for their valuable discussions throughout this research.

3.7 References

[1] Tjong SC. *Mater Sci Eng R* **53**, 73, (2006).

[2] Coleman JN, Khan U, Gun'ko YK. *Adv Mater* **18**, 689 (2006).

[3] Coleman JN, Khan U, Blau WJ, Gun'ko YK. *Carbon* **44**, 1624, (2006).

[4] Gao J, Itkis ME, Yu A, Bekyarova E, Zhao B, Haddon RC. *J Am Chem Soc* **127**, 3847, (2005).

[5] Liu T, Phang IY, Shen L, Chow SY, Zhang W. *Macromolecules* **37**, 7214 (2004).

[6] Jeong W, Kessler MR. *Chem Mater* **20**, 7060, (2008).

[7] Lynn DM, Kanaoka S, Grubbs RH. *J Am Chem Soc* **118**, 784, (1996).

[8] Weck M, Jackiw JJ, Rossi RR, Weiss PS, Grubbs RH. *J Am Chem Soc* **121**, 4088, (1999).

[9] Trnka M, and Grubbs RH. *Acc Chem Res* **34**, 18, (2001).

[10] Sheng X, Kessler MR, Lee JK. *J Therm Anal Calorim* **89**, 459, (2007).

[11] Thostenson ET, Chou T. *J Phys D Appl Phys* **36**, 573, (2003).

[12] Zhang X, Liu T, Sreekumar TV, Kumar S, Moore VC, Hauge RH, Smallley, RE. *Nano Lett* **3**, 1285, (2003).

[13] Gojny FH, Wichmann MHG, Kopke U, Fiedler B, Schulte K. *Compos Sci Technol* **64**, 2363, (2004).

[14] Liu L, Barber AH, Nuriel S, Wagner HD. *Adv Funct Mater* **15**, 975, (2005).

[15] Xie S, Li W, Pan Z, Chang B, Sun L. *J Phys Chem Solids* **61**, 1153, (2000).

[16] Salvetat JP, Kulik AJ, Bonard JM, Briggs AD, Stockli T, Metenier K, Bonnamy S, Beguin F, Burnham NA, Forro L. *Adv Mater* **11**, 161, (1999).

[17] Crosby AJ, Lee JY. *Polymer Reviews* **47**, 217, (2007).

[18] Rittingstein P, Priestley RD, Broadbelt LJ, Torkelson JM, *Nat Mater* **6**, 278, (2007).

CHAPTER 4: BIO-BASED RUBBERS BY CONCURRENT CATIONIC AND RING OPENING METATHESIS POLYMERIZATION OF MODIFIED LINSEED OIL

A paper to be submitted to *Macromolecular Rapid Communications*

Wonje Jeong[1], Timothy C. Mauldin[1], Richard C. Larock[2], Michael R. Kessler[1,3]

4.1 Abstract

Bio-based polymers prepared by tandem cationic polymerization and ring-opening metathesis polymerization (ROMP) using a norbornenyl-modified linseed oil, Dilulin™, and a norbornene diester, di-decyl-5-norbornene-*endo*-2,3-dicarboxylate (NBDC), have been prepared and characterized. Increasing concentration of the NBDC in Dilulin results in a decrease of glass transition temperature. The new bio-based polymers exhibit tensile test behavior ranging from relatively brittle (18 % elongation) to increased elongation (52 %) and decreased values of tensile stress with increasing NBDC content. Thermogravimetric analysis reveals that the bio-based rubbers have maximum decomposition temperatures of over 450 °C with thermal stability decreasing with increasing loadings of NBDC.

---

[1]Graduate student, Graduate student, and Assistant Professor, respectively, Department of Materials Science and Engineering, Iowa State University.

[2] Professor, Department of Chemistry.

[3] Author for correspondence.

4.2 Introduction

In recent decades bio-based polymers have attracted much attention as viable alternatives to petroleum-based plastics and offer the potential of biodegradability after use. Expanding the use of such biorenewable polymers, which have been shown to have properties comparable to widely used industrial plastics and elastomers, can partially reduce dependency on the petroleum-based feedstock used in the production of commercial polymers. Biorenewable polymers are typically derived from natural oils, starches, or proteins [1].

Vegetable oils are generally triglyceride structures with three fatty acids connected to a glycerol center. The fatty acids vary from 16 to 18 carbons in length, with 0 to 3 carbon double bonds resulting in different degrees of unsaturation. Substantial improvements in the field of biopolymers derived from soybean [2-7], corn [8], tung [9,10], linseed [11-13], fish [14,15], and castor oil [16-18] have been reported over the last decade with different types of polymerization: cationic [19-21], free radical [22,23], thermal [24,25], and ring-opening metathesis polymerization (ROMP) [26-28]. Cationic copolymerization of the soybean oil with divinylbenzene, styrene, and dicyclopentadiene initiated by boron trifluoride diethyl etherate (BF_3•OEt_2) results in polymers ranging from soft rubbers to hard thermosets with good mechanical properties and thermal stability [4-6]. Also reports of biopolymers resulting from ring-opening metathesis polymerization have recently appeared in the literature. ROMP of a functionalized castor oil and cyclooctene results in rubbery thermosets [26], and the ROMP of a cyclopentadiene-modified linseed oil and dicyclopentadiene results in a unique, strong biopolymer [27]. The addition of a bifunctional cross-linker in the same

cyclopentadiene-modified linseed oil results in a glassy thermoset biopolymer with a high glass transition temperature [28].

Herein, we focus on developing bio-based rubbers as a potential replacement for synthetic rubbers used in industrial applications. Requirements of elastomers for engineered materials such as tires, seals, and gaskets are high elongation and glass transition temperatures considerably lower than working temperatures [29-31]. Vegetable oil-based rubber appears promising in meeting the elongation requirements for these applications, as recent research reported that elastomers with elongation strains of over 300 % can be achieved by cationic polymerization of soybean oil with styrene [5], which is impressive considering biopolymers using vegetable oils are typically brittle relative to butadiene-based commercial rubbers due to low degrees of unsaturation in the triglyceride fatty acid molecule. However many approaches to copolymerizing vegetable oils with commercial petroleum-based resins (e.g. styrene and divinylbenzene) result in networks with glass transition temperatures that are too high for traditional rubber applications [2,4].

In this work, we develop bio-based polymers using norbornenyl functionalized linseed oil along with a norbornene diester derivative, di-decyl-5-norbornene-*endo*-2,3-dicarboxylate (NBDC) by combination of cationic and ring-opening metathesis polymerization. The flexible NBDC comonomer is added to provide increased elongation and to lower the glass transition temperature of the rubber. The thermal and mechanical properties of these new bio-based rubbers are determined by tensile testing, dynamic mechanical analysis (DMA), and thermogravimetric analysis (TGA).

The uniqueness of these rubbers is that they uses both ROMP and cationic polymerization to achieve higher levels of crosslinking. Both ROMP and cationic

polymerization are a chain growth processes. However, in ROMP the mechanism of the polymerization is based on olefin metathesis, with a unique metal-mediated carbon-carbon double bond exchange process as the cyclic olefin is converted to a polymeric material [32]. As a result, any unsaturation associated with the monomer is conserved as it is converted to polymer. By using a ROMP catalyst that reacts at a lower temperature than the cationic initiator, a polymer can be designed to first react in a way that does not change the degree of unsaturation, and allows some defined polymer to be formed, while the number of "reactive sites" for cationic polymerization is unchanged.

4.3 Experimental

4.3.1 Materials

Dilulin™ is a commercially available oil from Cargill (MN, USA) and synthesized by the Diels-Alder reaction at high temperatures and pressures between linseed oil and dicyclopentadiene [26], which decomposes to two cyclopentadiene (CPD) molecules at elevated temperature. Dilulin™ appears to be a 95:5 mixture of norbornyl-functionalized linseed oil and unreacted CPD oligomers and possesses an average of less than one bicyclic moiety per triglyceride [27]. Dilulin™ was obtained from Cargill and used as received without further purification and stored in a refrigerator. The chemical structure of Dilulin is shown in Figure 4-1. Maleic anhydride, dicyclopentadiene, and decanol were used for the synthesis of NBDC and purchased from Sigma-Aldrich and used as received. Second Generation Grubbs' catalyst (Benzylidene[1,3-bis(2,4,6-trimethylphenyl)-2-imidazolidinylidene]dichloro(tricyclohexylphosphine) ruthenium) was also purchased from Sigma-Aldrich. Since the size of Grubbs' catalyst affects the dissolution of the catalyst in the

resin [33], the catalyst was recrystallized by freeze-drying: 100 mg of Grubbs' catalyst was dissolved in 2 mL of benzene, flash-frozen in liquid nitrogen, and the benzene was allowed to sublime under vacuum for 24 hrs [28,34].

4.3.2 Synthesis of di-decyl-5-norbornene-endo-2,3-dicarboxylate

Maleic anhydride (168.3 g, 1.72 mol.) was dissolved in 1L of ethyl acetate in a 3-neck, 5L round-bottomed flask. Petroleum ether (1L) was added to this solution, and the flask was equipped with a reflux condenser and an addition funnel. While stirring, freshly distilled cyclopentadiene (170 ml, 2.06 mol.) was added dropwise at a rate of 5 ml/min. After addition of cyclopentadiene a white precipitate formed. Product was recrystallized from reaction solvent by heating until the precipitate dissolved, followed by slow cooling to 0 °C. Resulting product was vacuum filtered and dried under vacuum for 5 hours to reveal 238.8 grams of long, white crystals of nadic anhydride (85%). Purity = 99.5%, M.P. = 166.5°C, Endo/Exo = 99/1, ^{1}H NMR = (300 MHz/$CDCl_3$): δ 6.31 (t, 2H), 3.59 (dd, 2H), 3.51 (m, 2H), 1.78 (dt, 1H), 1.58(d, 1H). HRMS = Expected: 164.0473, Found: 164.0478.

Nadic anhydride (40.0 g, 0.24 mol.) was dissolved in 1L toluene in a 1-neck, 2L round-bottomed flask. To this solution was added 1-decanol (76g, 0.48 mol.), followed by slow addition of a catalytic amount of sulfuric acid, and the flask was equipped with a Dean-Stark apparatus. The solution was refluxed for 24 hours until a stoichometric amount of water was collected in the trap. After cooling, the reaction mixture was washed with water, dried with anhydrous $MgSO_4$, and the solvent was evaporated *in-situ* to reveal a clear, yellow liquid (106.0 g, 94%). Purity = ≥95%, Endo/Exo = 99/1, ^{1}H NMR = (300 MHz/$CDCl_3$): δ 6.22 (t, 2H), 3.96 (m, 4H), 3.25 (t, 2H), 3.13 (m, 2H), 1.55 (m, 4H), 1.45 (t, 1H), 1.43 (t, 1H), 1.24 (m, 28H), 0.86 (t, 6H). HRMS = Expected: 462.3709, Found: 462.3705. The overall

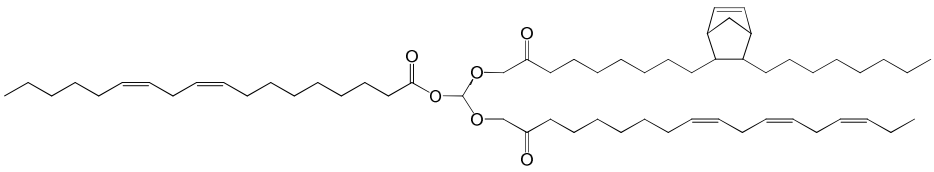

Figure 4-1 Chemical Structure of Dilulin.

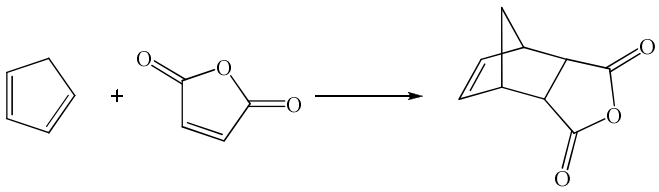

Figure 4-2a 5-norbornene-*endo*-2,3-dicarboxylic anhydride.

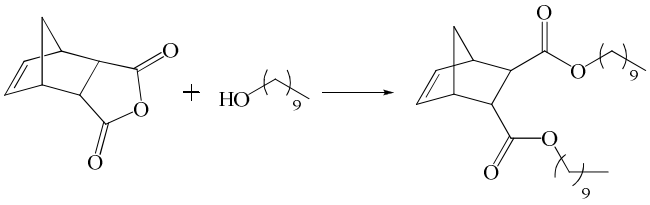

Figure 4-2b di-decyl-5-norbornene-*endo*-2,3-dicarboxylate.

schematic diagrams are shown in Figure 4-2.

4.3.3 Fabrication of bio-based rubbers

The bio-based rubbers have been prepared on a 20 g scale. Samples with three different loadings of NBDC (10, 20, and 30 wt %) were added to Dilulin and stirred 2 hrs for a homogeneous dispersion. Freeze-dried Grubbs' catalyst was then dissolved in solution (2 mg/g) by stirring, and degassed for 20 min under vacuum to remove entrapped air (generated during addition of Grubbs' catalyst) at which point the solution increased in viscosity. Then 3 wt % (based on the resin mixture) of cationic initiator, boron trifluoride diethyl etherate, was added under a nitrogen purge. After adding the cationic initiator, the mixture was stirred 5 min for homogeneous dispersion of catalyst and poured into a glass mold. The mold was then placed into a programmable oven and cured for 12 hr at 65 °C and 12 hr at 130 °C. The resulting polymer samples were dark brown. The nomenclature used here is as follows: Dilulin is referred to as Dil and di-decyl-5-norbornene-*endo*-2,3-dicarboxylate is referred to as NBDC. So a resin containing 70 wt % of Dilulin and 30 wt % of di-decyl-5-norbornene-*endo*-2,3-dicarboxylate is designated by Dil70-NBDC30. Dil(BFE) stands for Dilulin polymerized by cationic initiator and Dil(BFE,GC) for Dilulin polymerized by both cationic initiator and Grubbs' catalyst.

4.3.4 Characterization

Dynamic mechanical analysis (DMA, Q800 model, TA instruments) of the rubber composites was obtained in tension mode with sample dimensions of 2 mm thick and 5 mm width with an aspect ratio maintained at approximately 10. Each specimen was first cooled to about -100 °C and then heated at 3°C/min with a frequency of 1 Hz under nitrogen gas. The viscoelastic properties, the storage modulus E' and tan δ, were recorded as a function of

temperature. The glass transition temperatures (T_g) of the rubbers were obtained from the peaks of the tan δ curves. The tensile tests were conducted at 25 °C according to ASTM D638 (with type5 specimens) using an Instron universal testing machine (model 5569) equipped with a video extensometer at a crosshead speed of 2 mm/min. Thermogravimetric analysis (TGA, Q50 model, TA instruments) of the specimens was done on c.a. 20 mg of specimen under an air purge from room temperature to 650 °C at a heating rate of 10 °C/min.

4.4 Results and discussion

In general bio-based polymers of vegetable oils have intrinsically brittle properties because of their low unsaturation level. Therefore, we synthesized the diester derivative of norbornene, NBDC, which was reported to have both a low glass transition temperature (< -50 °C) and high elongation when polymerized (> 400 %) [35]. Our expectation is that during ROMP NBDC can copolymerize with Dilulin's norbornyl olefins, resulting in both increased elongation and decreased glass transition temperatures for the resulting polymer network.

The three different NBDC-containing samples (Dil90-NBDC10, Dil80-NBDC20, Dil70-NBDC30) employed in this study were polymerized by using two different types of catalyst; boron trifluoride diethyl etherate (BFE) for cationic polymerization and Grubbs' catalyst for ROMP. A detailed schematic illustration of the two polymerization mechanisms using two different types of initiators is shown in Figure 4-3. Figure 4-4 illustrates the temperature dependence of the storage modulus (E') for Dilulin with different loadings of NBDC. The Dil(BFE) sample shows typical storage modulus reduction for crosslinked polymer networks that are heated from the glassy state to the rubbery region above the glass

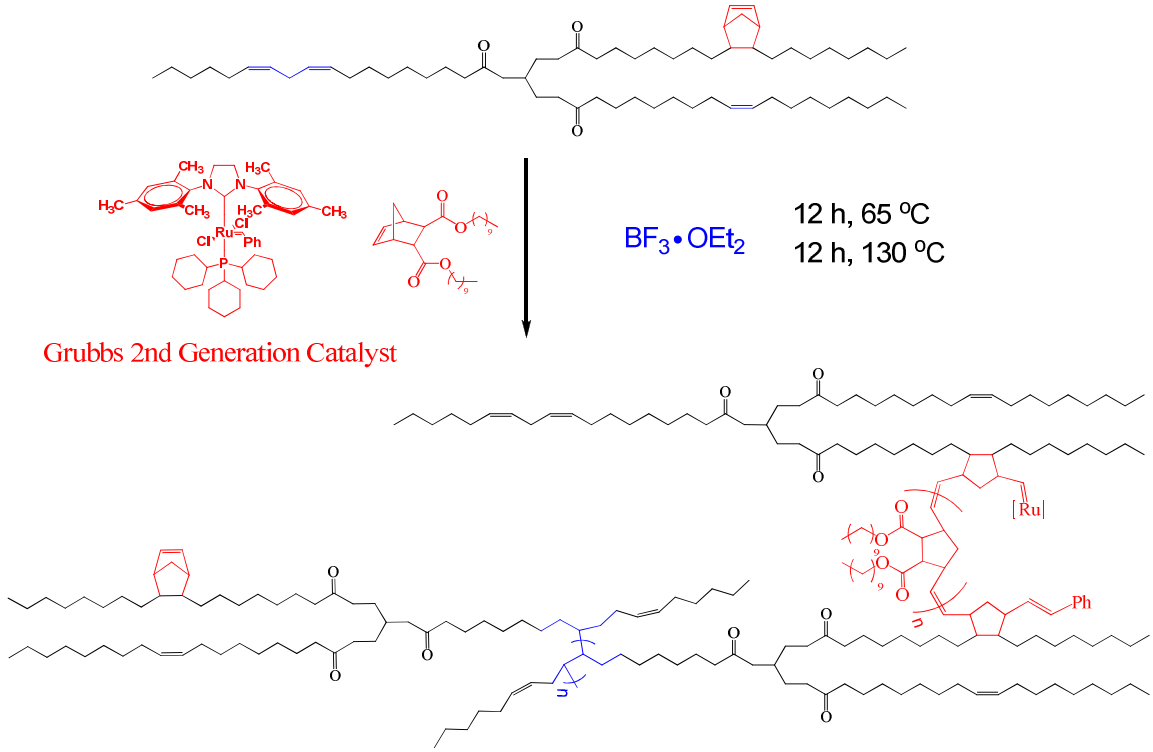

Figure 4-3 Schematic diagram of the combination of cationic polymerization and ring-opening metathesis polymerization using modified linseed oil with norbornene dicarboxylate.

transition temperature. The storage modulus remains nearly constant at low temperature and drops sharply in the temperature region between 0 to 20 °C, followed by a plateau at higher temperatures. The storage modulus of Dil(BFE, GC) is very similar to Dil(BFE), and the graph shifts approximately 2 to 3 °C higher, illustrating the effect of the ROMP of the norbornyl group in Dilulin on the overall thermal-mechanical properties. When NBDC was added to Dilulin the curves shifted to low temperatures and the storage modulus was decreased with increasing amounts of NBDC. From the theory of rubber elasticity, the crosslink density (ν_e) of a cross-linked polymer can be determined by the following equation [36,37,38].

$$E' = 3\,\nu_e RT \qquad (1)$$

Where E' is the storage modulus of the crosslinked polymer in the rubbery plateau region above T_g (T_g + 40 °C), R is the gas constant (8.314 J · K^{-1} · mol^{-1}), and T is the absolute temperature (K). The crosslink density of Dil(BFE), Dil70-NBDC30(BFE,GC), Dil80-NBDC20(BFE,GC), and Dil90-NBDC10(BFE,GC) were calculated to be approximately 390, 67.7, 22.2, 8.7 mol/m^3 respectively. The NBDC may be disrupting the cationic polymerization, such that the decrease in crosslink density is simply a result of higher loadings of non-crosslinkable NBDC and lower loadings of the crosslinkable Dilulin.

Figure 4-5 shows the temperature dependence of the loss factor tan δ for the Dilulin-based polymers with different weight percentages of NBDC. The tan δ peak temperature of Dil(BFE,GC) is 3 °C higher temperature than the Dil(BFE). With increasing loadings of NBDC, the glass transition temperature decreases from 8.6 °C to -5.7, -12.7, -17.4 °C respectively - a promising trend for bio-based polymers that have low glass transition temperatures. The T_g of Dilulin based polymers can be calculated by the Fox equation:

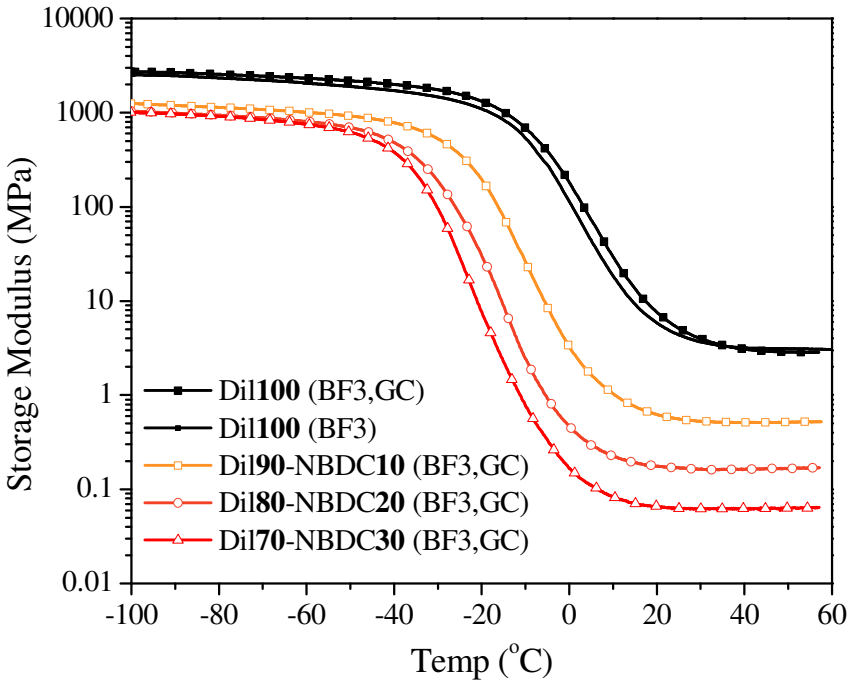

Figure 4-4 Temperature dependence of the storage modulus E' for Dilulin based polymers prepared with different weight percentage of NBDC.

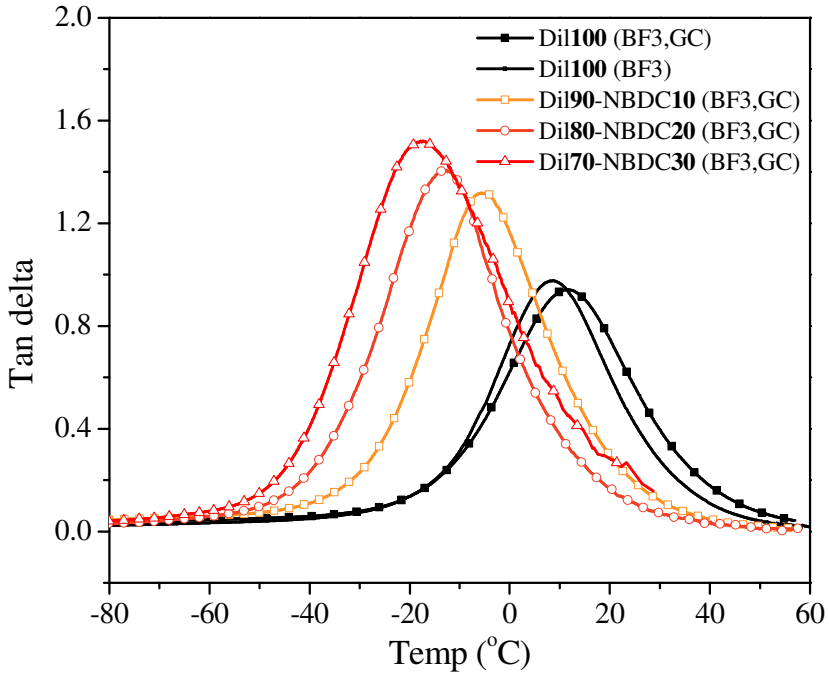

Figure 4-5 Temperature dependence of the tan δ for Dilulin based polymers prepared with different weight percentage of NBDC.

$$\frac{1}{T_g} = \frac{w_1}{T_{g1}} + \frac{w_2}{T_{g2}} \quad (2)$$

where T_{g1} and T_{g2} represent the glass transition of Dil(BFE,GC) and NBDC100; w_1 and w_2 are their mass fractions. The glass transition temperature of NBDC100 by ROMP is -55 °C (measured by DSC, data not shown). The calculated T_g values of the Dilulin/NBDC blends are 5 to 7 °C higher than the measured values (Table 4-1). This trend is expected for a material with higher crosslink density, as more crosslinking hinders the polymer's segmental motion, thus requiring higher temperatures for the onset of the glass transition. Samples with higher NBDC loadings also exhibit considerably higher tan δ values because of lower crosslinking densities and the linear NBDC polymer and oligomers not incorporated into the Dilulin matrix can act to plasticize the network. The height and area under the tan δ curve (shown in Table 4-1) gives an indication of the total amount of energy that can be absorbed by a material at a particular frequency. A large area under the tan δ curve indicates a great degree of molecular mobility, meaning it has better damping properties and can absorb and dissipate energy.

Tensile testing of Dilulin based Dil(BFE) polymer (Figure 4-6) shows tensile behavior typical of bio-rubbers that do not show ductile behavior. While the sample is not as brittle as a typical glassy thermoset, it shows low elongation compared to other rubbery materials. The tensile results of Dil(BFE,GC) polymer show 65% increase of modulus and 30 % increase of elongation, which suggests that the norbornyl group in Dilulin is reacting with Grubbs' catalyst by ROMP during curing. With increasing amounts of NBDC, the Young's modulus (from 0.38 to 0.08 MPa) and ultimate tensile strength (from 2.45 to 0.15 MPa) of the resulting polymers obviously decreases, and their elongation at break increases

Table 4-1 Dynamic mechanical analysis results for the Dilulin based polymers prepared with different weight percentage of NBDC.

	Dynamic Mechanical Analysis					
	E'_{-80}(MPa)[a]	E'_{30}(MPa)[b]	T_g (°C)[c]	T_g (°C)[d]	tan δ_{max}	TA(K)[e]
Dil**100** (BFE)	2333	3.67	8.6		0.97	34.9
Dil**100** (BFE,GC)	2558	3.96	11.6		0.94	37.5
Dil**90**-NBDC**10** (BFE,GC)	1139	0.53	-5.7	3.2	1.32	47.5
Dil**80**-NBDC**20** (BFE,GC)	942	0.16	-12.7	-4.8	1.40	50.6
Dil**70**-NBDC**30** (BFE,GC)	913	0.06	-17.4	-12.3	1.52	63.7

[a] Modulus at -80 °C
[b] Modulus at 30 °C
[c] Measured glass transition temperature measured by tan δ peak
[d] Calculated glass transition temperature by equation (2).
[e] tan δ area

(from 17.6 to 52 %). The elongation at break increases over 200 % compared to Dil(BFE) polymer.

Figure 4-7 shows the TGA data. The Dil(BFE) sample is thermally stable below 200 °C in air and exhibits three thermal decomposition stages above this temperature. The first stage degradation (200 – 420 °C) is attributed to evaporation and decomposition of the unreacted Dilulin and other soluble materials in the bulk sample. The second degradation stage (420 – 470 °C) is the fastest and corresponds to degradation and carbonization of the crosslinked polymer structure, while the last stage (> 470 °C) corresponds to gradual oxidation of the residue. Dil(BFE,GC) shows very similar thermal decomposition behavior to Dil(BFE) but 5 °C higher thermal stability, presumably due to the existence of additional crosslinking through ROMP of the norbornyl group on Dilulin, a presumption corroborated further by the DMA and tensile data. NBDC100, which is a linear ROMP polymer shows different thermal decomposition behavior compared to the neat Dilulin polymer. It starts to decompose about 200 °C and continuous to gradually decrease in weight until 350 °C, where a faster decomposition stage occurs until 400°C. Decomposition of char residue follows until all polymer residue is completely volatilized. When NBDC is added to Dilulin, the thermal decomposition phenomena is changed. The temperature of the first thermal decomposition stage decreases from 200 to 170 °C and the weight % of the second stage decreases from 85 to 62 % by adding up to 30 wt % NBDC. The linear NBDC polymer expected to be periodically bonded with the norbornyl group in the Dilulin may be decomposing between 200 to 320 °C, which is a slightly lower temperature than the rapid thermal decomposition of neat NBDC polymer. However this trend is reasonable considering

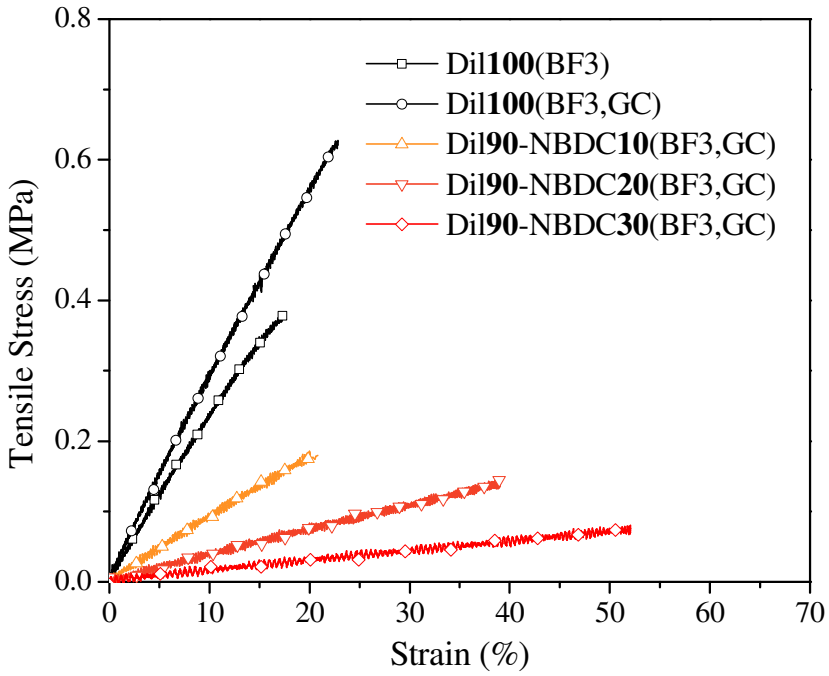

Figure 4-6 Tensile stress-strain curves for Dilulin based polymers prepared with different weight percentage of NBDC.

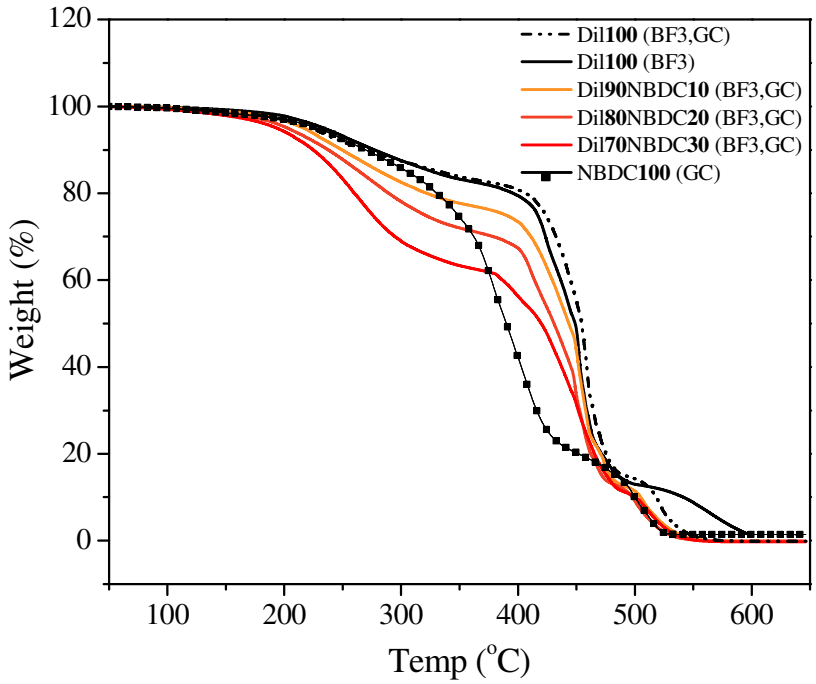

Figure 4-7 Thermogravimetric analysis of the Dilulin based polymers prepared with different weight percentage of NBDC.

Table 4-2 Tensile test and thermogravimetric results for the Dilulin based polymers prepared with different weight percentage of NBDC.

	Tensile Test			TGA data (°C)	
	σ (MPa)	***E*** (MPa)	ε_B (%)	T_{10}[a]	T_{50}[b]
Dil**100** (BFE)	0.38	2.45	17.6	277.2	448.9
Dil**100** (BFE,GC)	0.63	2.97	22.9	269.2	454.3
Dil**90**-NBDC**10** (BFE,GC)	0.18	0.91	20.8	249.4	443.6
Dil**80**-NBDC**20** (BFE,GC)	0.14	0.38	37.5	237.6	430.9
Dil**70**-NBDC**30** (BFE,GC)	0.08	0.15	52.0	224.6	419.9
NBDC**100** (GC)				269.5	390.0

[a] 10 % weight loss temperature

[b] 50 % weight loss temperature

the polymerized NBDC in Dilulin ought to be shorter in chain length compared to 100 % NBDC linear bulk samples polymerized by ROMP.

4.5 Conclusions

Bio-based polymers prepared from a norbornyl functional group-modified linseed oil is reported. A diester derivative of norbornene, di-decyl-5-norbornene-*endo*-2,3-dicarboxylate (NBDC), was synthesized, which could react via ROMP with the norbornyl functional groups in Dilulin during polymerization. Both cationic initiator and Grubbs' catalyst were used in tandem for fabricating these bio-based polymers. Dynamic mechanical analysis demonstrated that the glass transition temperature of the Dilulin/NBDC polymer decreased from 8 to -17 °C with increasing NBDC content, in accordance with calculated values. TGA analysis shows that all of the samples are thermally stable below 200 °C and thermal stability decreases with increasing NBDC content.

4.6 Acknowledgment

The authors thank Professor Sriram Sundararajan, Professor Sungho Yoon, Marlen Valverde, and Satyam Bhuyan for helpful discussions Financial support from the University of Northern Iowa Recycling Reuse Technology Transfer Center and the Plant Sciences Institute at Iowa State University is gratefully acknowledged.

4.6 References

[1] Wool RP, Sun XU. Bio-Based Polymers and Composites; Elsevier: Chapter 1 (2005).

[2] Li F, Hanson MV, Larock RC. *Polymer* **42**, 1567, (2001).

[3] Li F, Larock RC. *J Appl Polym Sci* **80**, 658, (2001).

[4] Li F, Larock RC. *J Polym Sci B Polym Phys* **38**, 2721, (2000).

[5] Li F, Larock RC. *J Polym Sci B Polym Phys* **39**, 60, (2001).

[6] Li F, Larock RC. *Polym Adv Technol* **13**, 436, (2002).

[7] Li F, Larock RC. *J Appl Polym Sci* **84**, 1533, (2002).

[8] Li F, Hasjim J, Larock RC. *J Appl Polym Sci* **90**, 1830, (2003).

[9] Li F, Larock RC. *J Appl Polym Sci* **78**, 1044, (2000).

[10] Li F, Larock RC. *Biomacromolecules* **4**, 1018, (2003).

[11] Tuman SJ, Chamberlain D, Scholsky KM, Soucek MD. *Prog Org Coat* **28**, 251, (1996).

[12] Gultekin M, Beker U, Guner FS, Erciyes AT, Yagci Y. *Macromol Mater Eng* **283**, 15, (2000).

[13] Akbas T, Beker UG, Guner FS, Erciyes AT, Yagci Y. *J Appl Polym Sci* **88**, 2373, (2003).

[14] Li F, Larock RC, Otaigbe JU, *Polymer* **41**, 4849, (2000).

[15] Marks DW, Li F, Pacha CM, Larock RC. *J Appl Polym Sci* **81**, 2001, (2001).

[16] Kumar VG, Venkatachalam S, Rao KVC. *J Polym Sci Polym Chem* **22**, 2317, (1984).

[17] Cassidy PE, Schwank. *J Appl Polym Sci* **18**, 2517, (1974).

[18] Ashraf SM, Ahmad S, Riaz U, Sharma HO. *J Appl Polym Sci* **100**, 3094, (2006).

[19] Warwel S, Bruse F, Demos C, Kunz M, Rusch gen Klass M. *Chemosphere* **43**, 39, (2001).

[20] Patel J, Mujcinovic S, Jackson WR, Robinson AJ, Serelis AK, Such C. *Green Chem* **8**, 450, (2006).

[21] Khot SN, Lascala JJ, Can E, Morye SS, Williams GI, Palmese GR, Kusefoglu SH, Wool RP. *J Appl Polym Sci* **82**, 703, (2001).

[22] Frankel EN. *Prog Lipid Res* **19**, 1, (1980).

[23] Valverde M, Andjelkovic DD, Kundu PP, Larock RC. *J Appl Polym Sci* **107**; 423, (2008).

[24] Wang C, Erhan S. *J Am Oil Chem Soc* **76**, 1211, (1999).

[25] Kundu P, Larock RC. *Biomacromolecules* **6**, 797, (2005).

[26] Henna PH, Larok RC. *Macromol Mater Eng* **292,** 1201, (2007).

[27] Henna PH, Kessler MR, Larock RC. *Macromol Mater Eng* **293**, 979, (2008).

[28] Mauldin TC, Haman K, Sheng X, Henna PH, Larock RC, Kessler MR. *J Polym Sci A Polym Chem* **46**, 6851, (2008).

[29] Wang MJ et al. Rubber *Chemistry and Technology* **75**, 247, (2002).

[30] Byers JT *Rubber Chemistry and Technology* **75**, 527, (2002).

[31] Wang MJ, Zhang P, Mahmud K. *Rubber Chemistry and Technology* **74**, 124, (2001).

[32] Calderon N. Olefin metathesis reaction. *Acc. Chem. Res.* **5**, 127, (1972).

[33] Jones AS, Rule JD, Moore JS, White SR, Sottos NR. *Chem. Mater.* 2006, **18**, 1312.

[34] Wilson GO, Caruso MM, Teimer NT, White SR, Sottos NR, Moore JS. *Chem Mater* **20**, 3288, (2008).

[35] Patent FR 1556215.

[36] Ward IM, Mechanical Properties of Solid Polymer; Wiley Interscience: London; Chapter 5; (1971).

[37] Murayama T, Dynamic mechanical analysis of Polymeric Materials; Elsevier: Amsterdam, (1978).

[38] Nielsen LE, Landel RF, Mechanical Properties of Polymers and Composites, 2nd ed.; Marcel Dekker: New York; Chapter 4; (1994).

CHAPTER 5: GENERAL CONCLUSIONS

5.1 General conclusions

The first topic reports on the synthesis and characterization of novel composite materials reinforced with MWCNTs by ring-opening metathesis polymerization (ROMP) using two ROMP based monomers: DCPD and ENB.

First, low loadings for MWCNT/polyDCPD composites are developed. Homogeneous dispersion of MWCNTs in polyDCPD was achieved by grafting norbornene functional group onto the nanotube surface. The investigation of mechanical properties of the composites resulted in a remarkable increase of tensile toughness (925% increase over the neat polyDCPD) with just 0.4 wt % of functionalized MWCNTs (f-MWCNTs). Dynamic mechanical analysis shows that there is a general increase of thermal stability (T_g) with the addition of f-MWCNTs, which means that covalently bonded f-MWCNTs can reduce the mobility of the matrix by interfacial interactions resulting in a distinctive increase of T_g of the composites. Traditional methods for toughening thermosetting polymers with toughening agents typically come at the expense of other properties such as modulus, strength, or decreasing thermal stability. However, the system described here substantially increases the toughness, while at the same time increases the glass transition temperature using f-MWCNTs via ROMP.

With the second monomer system, ENB is polymerized by ROMP to produce a linear thermoplastic polymer. The differences between DCPD and ENB are the number of ROMP active double bonds and curing kinetics, with the ENB being significantly more reactive than

the endo-DCPD. Using the same f-MWCNTs developed for the DCPD system, we investigated the effectiveness of f-MWCNTs on the thermo-mechanical properties of thermoplastic polyENB. Like the DCPD nanocomposites, significant enhancement of the toughness of polyENB composites is obtained at with a low loading (0.8 wt %) of f-MWCNTs. The huge increased elongation indicates that the ROMP approach for polyENB is also very effective.

The figure 5-1 illustrates the comparison of the toughness efficiencies (change in toughness normalized with f-MWCNTs loading) in the polyDCPD and polyENB system with increasing f-MWCNTs loadings. As shown in figure 5-1, toughness change in polyDCPD system follows linear increase. In the polyENB system there is a scattering of data however the elongation increases over 100 % (both 0.8 and 1.6 wt % f-MWCNTs samples) and results in dramatic morphological change in gauge regions after break shown in figure 3-5. In terms of Young's modulus, both systems give no noticeable improvements compared to toughness, which can be assumed because of the shorten f-MWCNTs.

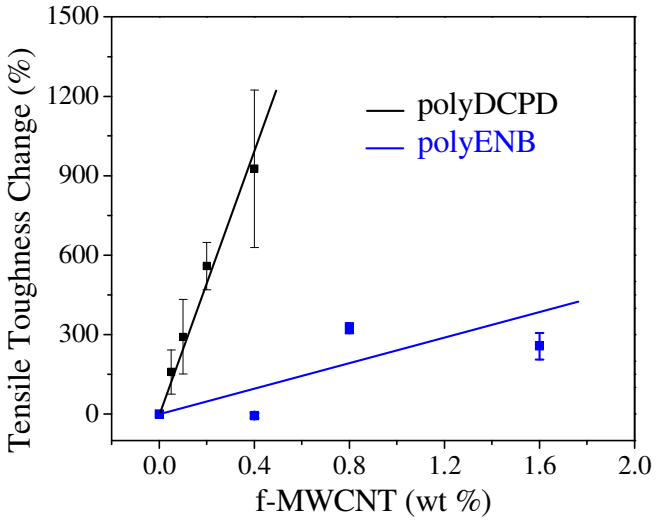

Figure 5-1 Comparison of the toughness efficiencies in the polyDCPD and polyENB system with increasing f-MWCNTs loadings.

5.2 Recommendations for future research

The motivation of the research about MWCNTs reinforced both polyDCPD and polyENB composites came from self-healing research. As discussed the introduction in chapter 2, self-healing system has been focused on restoring the mechanical properties of structural materials. Both DCPD and ENB monomer have been used in self-healing system, where they were kept in microcapsule and embedded in the matrix. As discussed in chapter 2, in f-MWCNTs/polyDCPD systems, impressive results of mechanical properties can be obtained only 0.4 wt % (~ 0.17 Vol. %) of f-MWCNTs loading, which is very little amount compared to commercial micro-scale fillers. Such a low wt % of f-MWCNTs loading, the stabilized dispersion of f-MWCNTs/DCPD solution has relatively low viscosity suitable for fabricating microcapsules. Therefore it would be beneficial for verifying the suitability of f-MWCNTs for self-healing system.

Thermomechanical properties of bio-based rubbers using norbornenyl-modified linseed oil with diester derivatives by have been investigated by tandem cationic polymerization and ROMP. However we expect that the real tandem polymerization mechanisms would be more complicated than we discussed such that more detail analyses would be need for example curing kinetics and in-situ NMR analysis about catalyst activity.